Bounded control of an underactuated biomimetic aerial vehicle - Validation with robustness tests

Hala Rifai, Nicolas Marchand, Guylaine Poulin-Vittrant

▶ **To cite this version:**

Hala Rifai, Nicolas Marchand, Guylaine Poulin-Vittrant. Bounded control of an underactuated biomimetic aerial vehicle - Validation with robustness tests. Robotics and Autonomous Systems, 2012, 60 (9), pp.1165-1178. 10.1016/j.robot.2012.05.011 . hal-00675527

HAL Id: hal-00675527
https://hal.science/hal-00675527

Submitted on 1 Apr 2012

HAL is a multi-disciplinary open access archive for the deposit and dissemination of scientific research documents, whether they are published or not. The documents may come from teaching and research institutions in France or abroad, or from public or private research centers.

L'archive ouverte pluridisciplinaire **HAL**, est destinée au dépôt et à la diffusion de documents scientifiques de niveau recherche, publiés ou non, émanant des établissements d'enseignement et de recherche français ou étrangers, des laboratoires publics ou privés.

hal-00675527, version 1 - 1 Mar 2012

Bounded control of an underactuated biomimetic aerial vehicle - Validation with robustness tests ☆

Hala Rifaï[a], Nicolas Marchand[b], Guylaine Poulin-Vittrant[c]

[a] *LISSI, EA 3956 - University of Paris-Est Créteil, 122 rue Paul Armangot, 94400 Vitry-Sur-Seine, FRANCE*
[b] *GIPSA-lab, Control Systems Department, UMR CNRS 5216-INPG-UJF, ENSIEG BP 46, 38402 Saint Martin d'Hères Cedex, FRANCE*
[c] *LEMA, UMR 6157 CNRS-CEA - University François Rabelais de Tours, Site de Blois, Rue de la Chocolaterie, 41000 Blois, FRANCE*

Abstract

Flapping wing Micro Aerial Vehicles (FMAVs) have recently emerged as a promising challenge lying on the progress of the avionics technologies. The present paper deals with the development of simple control laws for an embedded implementation on a biomimetic MAV, aiming to control its attitude and position. The control laws are bounded, taking into consideration the amplitude bounds of the control angles characterizing the flapping wings movement. In order to validate the control laws, a simplified model having a simple wing kinematic parametrization and considering only the main aerodynamic forces and torques is proposed. The stability of the controller is shown in simulations using a diptera insect model. The robustness of the proposed controller is emphasized through different robustness tests. They concern mainly external disturbances, model and aerodynamic parameters errors, and aim to validate the considered simplifications in the model.

Keywords: Flapping flight, bounded control, averaging, modeling.

☆This work is part of OVMI/EVA projects, supported by the French National Research Agency (ANR).

Email addresses: hala.rifai@u-pec.fr (Hala Rifaï), nicolas.marchand@gipsa-lab.grenoble-inp.fr (Nicolas Marchand), guylaine.poulin-vittrant@univ-tours.fr (Guylaine Poulin-Vittrant)

hal-00675527, version 1 - 1 Mar 2012

1. Introduction

Since many decades, the flapping flight mechanisms have been an investigation field for biologists and aerodynamicists. Their research has come to fruition; recent results, even if relatively immature, have attracted the avionics, robotics and control communities allowing to build aerial vehicles able to mimic the nature's flight patterns.

Flapping wing Micro Aerial Vehicles (FMAVs) aim to combine the advantages of the rotary and fixed airfoils [1]. They have a great maneuverability, develop high lift, and theoretically consume low energy. Moreover, they produce soft noise and get benefit of their biomimetic shape and behavior to execute discrete missions. The major disadvantages are still the difficulty to identify the mechanisms developed by insects during complex maneuvers [2] and to reproduce these movements [3]. Moreover, the conventional aerodynamic theory, well known for fixed airfoils, fails for flapping airfoils due to the low Reynolds numbers and the influence of the unsteady airflows on the wings besides the high degrees of under actuation. Even if autonomous flight is still far from being achieved, the progress in microelectronic technology (sensors, actuators, processors, batteries), materials (body and wings membranes), communication tools, etc. is helping researchers to develop prototypes capable of flapping flight. FMAVs may be used for numerous indoor and outdoor civil applications (supervision of buildings and forests, inspection of high monuments, intervention in narrow and dangerous environments for rescuing, games), military applications (espionage and investigation) or even for the exploration of other planets.

The objective of this paper is to achieve the control of a FMAV's position and orientation, by controlling indirectly the amplitudes of its wing angles. Note that, within a biological scope, the wing angle amplitudes are bounded. Moreover, from a technical point of view, the actuators driving the wings deliver a limited power. These constraints have motivated the development of bounded force and torque control laws. The wing angle amplitudes are deduced using the averaged model over a wingbeat period, then are applied to the time varying system. This strategy is efficient for high-frequency oscillating systems like flapping-wing MAVs: the aerodynamic forces and torques, generated by the wings, affect the FMAV's behavior only by their mean values since the body's dynamics are much slower than the flapping wings ones. The control laws are then applied to a simple model of a FMAV, representing a diptera insect of $200\,mg$ capable of hovering flight. Different

hal-00675527, version 1 - 1 Mar 2012

robustness tests are achieved to validate the considered simplifications and to fill in the lack of experimentations on an autonomous and instrumented prototype.

Attitude stabilization of flapping airfoils has been treated in the literature using the linearized dynamics of the system to compute a Proportional Derivative controller [4], state feedback controllers [5, 6] that can be based on poles placement [7] or based on a dynamic estimation of system's states [8] and a Linear Quadratic Gaussian (LQG) optimal control [7]. The control in three dimensions has been treated in [9] using a state feedback controller acting directly on the position. A bounded state feedback of the vertical force and torques has been developed in [7], this control is computed using the linearized dynamics of the system and is based on poles placement. A LQG is also designed in [10]. A new strategy consists on passively regulating the body's torques using an adaptable mechanical structure of the wings [11]. All these controls act on the wing angle amplitudes and are based on the averaged dynamics of the system. A first study has exploited the control of the frequency and phase difference of wing angle [12] but the control of the FMAV in the 3D space has not been achieved yet. One should note that all these works are tested only by simulations. First prototypes of FMAVs, at micro scale, are still not capable of autonomous flight [13, 14, 15, 16]. The stabilization of the vertical movement has been achieved and tested experimentally in [17], the FMAV is however attached by wires to avoid any rotational movement. One should also note that in some of the aforementioned works, the control is built upon output feedback. However, the control laws are linear, computed around the equilibrium. Therefore, they are only locally stable and consequently, structurally not sufficiently robust with respect to external disturbances like rain drops, system uncertainties (like inertia parameters, geometry, etc.) or physical bounds of the system. The present work considers that all states are accessible (measurable or estimated). Future works will treat the case of controlling the system using directly sensors measurements. The proposed state feedback control laws have the particularity of almost globally stabilizing the position and orientation of the flapping aerofoil using bounded control based on nested saturations with poles placement. This allows to respect the saturation of the actuators driving the flapping wings and to accelerate the convergence. The control is also shown to be robust with respect to external disturbances and system modeling or aerodynamic errors.

The paper is organized as follows. In section 2, some definitions and

hal-00675527, version 1 - 1 Mar 2012

notations are given. Section 3 details the model of the FMAV: wings degrees of freedom and body's dynamics. In section 4, simple bounded control laws are developed in order to stabilize the position and orientation of the FMAV. Application to a simplified model is presented in section 5 aiming to validate the control laws. The robustness of the control with respect to the model simplifications, disturbances, aerodynamic errors, etc. are emphasized in section 6. Finally, conclusions are presented in section 7.

2. Notations and preliminary definitions

An integrator chain of order $n \in \mathbb{N}$ is defined by:

$$\left\{ \begin{array}{rcll} \dot{x}_i & = & x_{i+1} & \text{for } i \in \{1, \ldots, n-1\} \\ \dot{x}_n & = & u & \end{array} \right. \tag{1}$$

u is the control input.

A classical sign$(\cdot)$ function is defined by:

$$\text{sign}(x) \;=\; \left\{ \begin{array}{ll} 1 & \text{if } \; x \geq 0 \\ -1 & \text{if } \; x < 0 \end{array} \right. \tag{2}$$

A classical saturation function $\text{sat}_M(\cdot)$ is defined by:

$$\text{sat}_M(x) \;=\; \left\{ \begin{array}{ll} x & \text{if } \; |x| \leq M \\ M\text{sign}(x) & \text{if } \; |x| > M \end{array} \right. \tag{3}$$

with M the saturation bound.

A twice differentiable saturation function $\sigma_M(\cdot)$ bounded between $\pm M$, $M > 0$, and parameterized by $0 < \mu < 1$ can be defined as $\sigma_M(\cdot) = M\sigma(\cdot)$, with $\sigma(\cdot)$ bounded between ± 1 and expressed by:

$$\sigma(x) = \left\{ \begin{array}{ll} -1 & x < -1-\mu \\ e_1 x^2 + e_2 x + e_3 & x \in [-1-\mu, -1+\mu[\\ x & x \in [-1+\mu, 1-\mu] \\ -e_1 x^2 + e_2 x - e_3 & x \in]1-\mu, 1+\mu] \\ 1 & x > 1+\mu \end{array} \right. \tag{4}$$

with $e_1 = \frac{1}{4\mu},\ e_2 = \frac{1}{2} + \frac{1}{2\mu},\ e_3 = \frac{\mu^2 - 2\mu + 1}{4\mu}$.

hal-00675527, version 1 - 1 Mar 2012

A level function $\gamma(\cdot,\cdot,\cdot)$ associated to an integrator chain is defined by [18]:

$$\gamma_i(x_{i+1}, L_{i+1}, M_i) = \begin{cases} M_i & \text{if} \quad |x_{i+1}| > L_{i+1} \\ M_i + L_{i+1} - |x_{i+1}| & \text{if} \quad |x_{i+1}| \leq L_{i+1} \end{cases} \tag{5}$$

with $M_i := L_{i+1}$ for $i \in \{1, \ldots, n-1\}$ and $L_i := M_i$ for $i \in \{2, \ldots, n\}$, n corresponds to the integrator chain order and $L_n = u$.

$\bar{x}$ denotes the average of x over a wingbeat period.

3. Flapping flight modeling

A FMAV consists of two main parts: the flapping wings and the body.

3.1. Wing's degrees of freedom

A flapping wing has four degrees of freedom: feathering, flapping, lagging and spanning (Figure 1). The feathering is a rotation of the wing along its span-wise axis, the flapping is an up and down movement of the wing, the lagging is a forward and backward movement of the wing parallel to the body and the spanning is an expansion and contraction of the wingspan. This last degree of freedom is not achievable by most of the insects. Furthermore, the wing is characterized by other complex phenomena like the flexion and the torsion [19]. Flexibility allows the wing to be more resistant to turbulence, provides a gentler flight and increases the aerodynamic force relative to a same size rigid wing [20]. Torsion allows the wing to twist and provides aerodynamic stability without the need of a tail. The first three degrees of freedom can be modeled respectively by three rotations of angles (ψ, ϕ, θ) about three axes $(\vec{r}, \vec{t}, \vec{n})$, defining a frame $\mathcal{R}^w(\vec{r}, \vec{t}, \vec{n}, \psi, \phi, \theta)$ attached to the wing at its base (Figure 2). Frames $\mathcal{R}^w$ are indexed left, $\mathcal{R}^w_l$, and right, $\mathcal{R}^w_r$, relative to the left and right wings. (ψ, ϕ, θ) are called respectively the rotation, flapping and deviation angles. The axis $\vec{r}$ is oriented from the wing base to its tip along the wingspan, the axis $\vec{t}$ is parallel to the wing chord, oriented from trailing to leading edge and the axis $\vec{n}$ is perpendicular to the wing plane oriented so that the three-sided frame $(\vec{r}, \vec{t}, \vec{n})$ is direct.

hal-00675527, version 1 - 1 Mar 2012

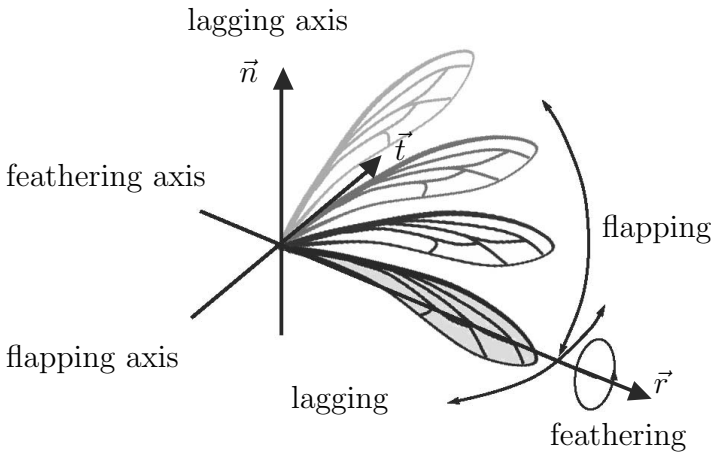

Figure 1: Degrees of freedom of a flapping wing

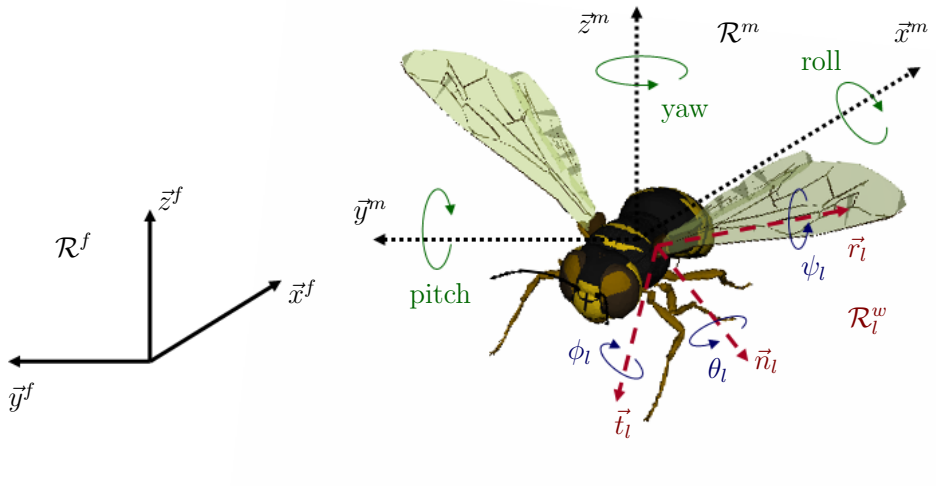

Figure 2: Coordinate frames and wing degrees of freedom

hal-00675527, version 1 - 1 Mar 2012

3.2. Body's dynamics

Let's first define a frame $\mathcal{R}^m(\vec{x}^m, \vec{y}^m, \vec{z}^m)$ attached to the FMAV's body at its center of gravity, and a frame $\mathcal{R}^f(\vec{x}^f, \vec{y}^f, \vec{z}^f)$ fixed in the space (Figure 2). Indexes m and f stand for mobile and fixed frames respectively.

The interaction of the flapping wings with the surrounding air generates the aerodynamic forces and torques. Besides, the insect's body is subject to viscous and gravitational forces. By a simple transformation, these forces and torques are projected in the mobile frame $\mathcal{R}^m$. The FMAV is considered as a rigid body subject to forces and torques. The latter are responsible of generating the FMAV's displacements and maneuvers. The motion of the body is computed through the dynamic equations:

$$\dot{P}^f = V^f \tag{6}$$

$$\dot{V}^f = \frac{1}{m} R^T(q) f^m - cV^f - g \tag{7}$$

$$\begin{pmatrix} \dot{q}_0 \\ \dot{q}_v \end{pmatrix} = \frac{1}{2} \begin{pmatrix} -q_v^T \\ I_3 q_0 - [q_v]^\times \end{pmatrix} \omega^m \tag{8}$$

$$\dot{\omega}^m = J_m^{-1}(\tau^m - \omega^m \times J_m \omega^m) \tag{9}$$

$P^f \in \mathbb{R}^3$ and $V^f \in \mathbb{R}^3$ are respectively the linear position and velocity of the body's center of gravity relative to the fixed frame $\mathcal{R}^f$. $\omega^m \in \mathbb{R}^3$ is the angular velocity with respect to the mobile frame $\mathcal{R}^m$. $c \in \mathbb{R}$ is the viscous coefficient and $g \in \mathbb{R}^3$ the gravity vector in $\mathcal{R}^f$. $f^m \in \mathbb{R}^3$ and $\tau^m \in \mathbb{R}^3$ are respectively the aerodynamic force and torque vectors defined in $\mathcal{R}^m$. $J_m \in \mathbb{R}^{3\times3}$ is the inertia matrix of the body relative to $\mathcal{R}^m$ and I_3 is the identity matrix. q is the quaternion defining the attitude of the body relative to $\mathcal{R}^f$ [21]:

$$q = [\cos\frac{\nu}{2} \ (\vec{e}^T \sin\frac{\nu}{2})]^T = [q_0 \ q_v^T]^T$$

consisting of a rotation of angle ν about the Euler axis $\vec{e}$. $q_0 \in \mathbb{R}$ is the scalar part and $q_v = [q_1 \ q_2 \ q_3]^T \in \mathbb{R}^3$ the vector part of the quaternion. $q \in \mathbb{H}$ where $\mathbb{H} = \{q \mid q_0^2 + q_v^T q_v = 1\}$ is the Hamilton space. $R(q) \in SO(3) = \{R(q) \in \mathbb{R}^{3\times3} : R^T(q)R(q) = I, \det R(q) = 1\}$ is the rotation matrix from the fixed frame $\mathcal{R}^f$ to the mobile frame $\mathcal{R}^m$. It is defined as:

$$R(q) = (q_0^2 - q_v^T q_v) I_3 + 2(q_v q_v^T + q_0 [q_v]^\times)$$

$[q_v]^\times$ is the skew symmetric matrix associated to q_v, given by:

$$[q_v]^\times = \begin{bmatrix} 0 & q_{v_3} & -q_{v_2} \\ -q_{v_3} & 0 & q_{v_1} \\ q_{v_2} & -q_{v_1} & 0 \end{bmatrix}$$

4. Flapping flight control

4.1. Control Strategy

Depending on the insects species, the wingbeat frequency ranges from a few Hertz to a few hundred Hertz [2]. The FMAV considered in this work is based on a diptera model having a high wingbeat frequency of $100\,Hz$. The FMAV falls therefore within the category of high frequency oscillating systems. The averaging theory [22, 23, 24] shows that the averaged dynamics of high frequency oscillating systems are a good approximation of the system's time varying dynamics. Therefore, the forces and torques, generated by the wings, affect the insect's movement only by their averaged values over a wingbeat period. Note that this strategy is widely use for the control of FMAVs [10, 25].

In this work, the amplitudes of the wing angles are chosen to be the control inputs. The wings are supposed to beat in the mean stroke plane, defined by taking the deviation angle θ to zero. Only two degrees of freedom per wing, e.g. the flapping and rotation angles, are considered. Consequently, only two actuators are needed per wing. This conception allows to simplify the FMAV's structure and notably decrease the on-board load. Denoting by $u = (\phi^l(t), \phi^r(t), \psi^l(t), \psi^r(t))$ the flapping and rotation angles for left and right wings, $v = (\phi_0^l, \phi_0^r, \psi_0^l, \psi_0^r)$ the amplitudes of the wing angles (19), then $u = v\, f_2(t)$.
Let $x = (P, V, q, \omega)$, the FMAV model detailed in (6-9) can be written in a compact form as:

$$\dot{x} = f_1(x, u) \tag{10}$$

Let $\bar{x} = (\bar{P}, \bar{V}, \bar{q}, \bar{\omega})$ denote the averaged state over a wingbeat period T. Averaging the FMAV's model over a wingbeat period and writing it in a compact form, one has:

$$\dot{\bar{x}} = \bar{f}_1(\bar{x}, v) \tag{11}$$

As mentioned previously, the averaged dynamics described by $\bar{f}_1$ are a good approximation of the oscillating dynamics given by f_1. The FMAV is con-

hal-00675527, version 1 - 1 Mar 2012

hal-00675527, version 1 - 1 Mar 2012

trolled indirectly by means of the wing angle amplitudes v that can be computed by a feedback of the system's averaged states:

$$v = h(\bar{x}) \tag{12}$$

If $\bar{x} = 0$ is an exponentially stable equilibrium point for the averaged system (11), then there exists $k > 0$ such that $\|x(t) - \bar{x}(t)\| < kT$ for all $t \in [0, \infty)$ which is motivating in the present case because the wingbeat period T is small.

In other words, a stable equilibrium state for the averaged dynamics of a high frequency oscillating system (11) is also a stable equilibrium state for the oscillating (time variant) system (10).

Remark 1. *One should emphasize that the averaging technique is used only to compute the control laws that should be applied to the FMAV and prove their stability; all the simulations and robustness tests are achieved using the high-frequency FMAV's model.*

As mentioned before, the amplitudes of the wing angles are chosen to be the control inputs. The relation between the angles defining the wings kinematics and the mean force and torque, averaged over a wingbeat period, can be written as:

$$(\bar{f}, \bar{\tau}) = \Lambda(\phi_0, \psi_0) \tag{13}$$

where $\bar{f}$ and $\bar{\tau}$ are respectively the averaged force and torque acting on the body, ϕ_0, ψ_0 are respectively the amplitudes of the flapping and rotation angles for the left and right wings. This relation can be found theoretically through mathematical equations (adopted in this work) or experimentally through some experiments and optimization strategies to define a mapping between the wing angle amplitudes and the measured aerodynamic forces.

The control strategy can be stated as follows:

1. Relatively to current and desired position and orientation, control torques and forces are computed using a state feedback $\mathcal{U}(\bar{x})$ approach for example.
2. Based on the averaging theory, these forces and torques are considered equal to the forces and torques that should be developed by the wings, averaged over a wingbeat period:

$$(\bar{f}, \bar{\tau}) = \mathcal{U}(\bar{x})$$

hal-00675527, version 1 - 1 Mar 2012

3. The wing angle amplitudes that should be applied at the beginning of a wingbeat period can then be deduced:

$$(\phi_0, \psi_0) = \Lambda^{-1}(\mathcal{U}(\bar{x}))$$

which satisfies system (12) with $h(\cdot) = \Lambda^{-1}(\mathcal{U}(\cdot))$.

In this paper, simple control laws are proposed in order to stabilize the position and attitude of the FMAV. The control design takes into consideration the saturation of the actuators. The choice of taking two degrees of freedom per wing allows to create roll and yaw rotations, besides longitudinal and vertical movements. Therefore, the FMAV belongs to the class of underactuated systems. In order to achieve a 3D movement in the space, the pitch and lateral controls should be realized. The pitch rotation will be controlled independently, considering a small mass moving inside the body and changing its center of gravity. This can be achieved technically using the ElectroWetting On Dielectric technology (EWOD) [26]. Note that insects use this technique by moving their legs or abdomen to change their center of gravity [2]. The rotational subsystem (8-9) becomes then fully actuated, and can be stabilized by applying control torques driving the roll, pitch and yaw angles (η_1, η_2, η_3) to zero. However, the translational subsystem (6-7) is still underactuated. The stability of this subsystem will be ensured for the longitudinal and vertical motions by applying control thrust $\bar{f}_x$ and lift $\bar{f}_z$, and for the lateral motion by tilting the FMAV sideway using the coupling between the roll and vertical movements. Note that this maneuver is accomplished by most of insects to achieve the lateral movement [2]. Therefore, system (6-9) will be considered as cascade of systems [27] since it is of the form:

$$\begin{cases} \dot{x} &= f(x, y) \\ \dot{y} &= g(y, u) \end{cases}$$

which means that the translational dynamics depend on the rotational ones, but the rotational dynamics are independent of the translational ones.

The asymptotic stability of the cascaded system's states $(x, y) = (0, 0)$ arises from the asymptotic stability of the equilibrium state, $x = 0$, of the first subsystem, driven by $y = 0$, and the asymptotic stability of the second subsystem equilibrium state $y = 0$ [28].

In the following, control torques and forces will be detailed.

hal-00675527, version 1 - 1 Mar 2012

4.2. Attitude control

A bounded state feedback control torque is proposed in order to stabilize the attitude of the FMAV. This control is based in its formulation on the model of a rigid body [29] (equivalent to the averaged model of the FMAV) and applied to the time varying model (FMAV). The control law is extremely simple, therefore suitable for an embedded implementation and consequently for an autonomous flight. Moreover, this control is robust with respect to aerodynamic errors and does not require the knowledge of the body's inertia. Let $\bar{\tau} = [\bar{\tau}_1, \bar{\tau}_2, \bar{\tau}_3]^T$ be the roll, pitch and yaw control torques.

$$\bar{\tau}_i = -\text{sat}_{M_{2,i}}(\lambda_i[\delta_i \bar{\omega}_i + \text{sign}(\bar{q}_0)\text{sat}_{M_{1,i}}(\rho_i \bar{q}_i)]) \tag{14}$$

with $i \in \{1, 2, 3\}$, sat and sign are defined respectively by (3, 2). $\text{sign}(\bar{q}_0)$ takes into account the possibility of 2 rotations (of angles ν and $2\pi - \nu$) to drive the body to its equilibrium orientation; the one of smaller angle is chosen. $\bar{\omega}_i$ and $\bar{q}_i$ are the averaged angular velocities and quaternion over a single wingbeat period representing the time varying angular velocities and quaternion of a rigid body. $\lambda_i,\ \delta_i,\ \rho_i$ are positive parameters. Differently from [29], δ_i has been added in order to slow down the convergence of the torque compared to the angular velocity such that it becomes physically achievable.

The asymptotic stability of the closed loop averaged system is proved in [29] (the added parameter δ_i does not change the proof).

Therefore, $\bar{\omega} \to 0$ and $\bar{q} \to 0$ (based on the rigid body case). By means of the averaging theory, $\|\omega - \bar{\omega}\| < k_1 T$ and $\|q - \bar{q}\| < k_2 T$ for $k_{1,2} > 0$ and T the wingbeat period.

An integrator can be added in the control law in order to eliminate any possible static error and to ensure more robustness of the system.

4.3. Position control

Neglecting the viscous force cV^f acting on the FMAV's body by assuming that it is moving at low speeds, the translational subsystem (6-7) can be transformed into a chain of integrators (1). cV^f will be considered as a disturbance term in simulations. Supposing that after a sufficiently long time, the FMAV is stabilized over the pitch and yaw axes ($\eta_2 = \eta_3 = 0$) thanks to the control law (14), thereby the rotation matrix defines solely a rotation about the roll axis $\vec{x}^m$. The normalized translational subsystem,

hal-00675527, version 1 - 1 Mar 2012

augmented of a state representing the integral of the position, can be written ($P^f = [P_x, P_y, P_z]^T$ is the current position):

$$\begin{cases} \dot{p}_1 &= p_2 \\ \dot{p}_2 &= p_3 \\ \dot{p}_3 &= v_x \end{cases} \tag{15}$$

$$\begin{cases} \dot{p}_4 &= p_5 \\ \dot{p}_5 &= p_6 \\ \dot{p}_6 &= -v_h \sin(\eta_1) \\ \dot{p}_7 &= p_8 \\ \dot{p}_8 &= p_9 \\ \dot{p}_9 &= v_h \cos(\eta_1) - 1 \end{cases} \tag{16}$$

$p = \frac{1}{g}(\overline{\int P}^f_x, \bar{P}^f_x, \bar{V}^f_x, \overline{\int P}^f_y, \bar{P}^f_y, \bar{V}^f_y, \overline{\int P}^f_z, \bar{P}^f_z, \bar{V}^f_z) = (p_1, \ldots, p_9)$ is the averaged state of the translational subsystem, $v_x = \frac{\bar{f}_x}{mg}$, $v_h = \frac{\bar{f}_z}{mg}$ with $\bar{f}_x$ and $\bar{f}_z$ are respectively the control thrust and lift, η_1 is the roll angle and 1 is the normalized gravity.
The averaged normalized system (15-16) will be used to compute the normalized control thrust v_x and lift v_h. As for (14), the proposed controls are bounded and are very simple to implement.

4.3.1. Stabilization of the forward movement (p_2, p_3)

System (15) defines a triple integrator. It can be stabilized using the control developed in [30] combining the amelioration proposed by [18, 31] in order to define variable bounds of the control laws and to accelerate their convergence by means of a pole placement at $\{-b_1, -b_2, -b_3\}$. Define the matrix Π:

$$\Pi = \begin{bmatrix} b_1 b_2 b_3 & b_3(b_1 + b_2) & b_3 \\ 0 & b_1 b_2 & b_2 \\ 0 & 0 & b_1 \end{bmatrix}$$

with $\Pi_{i,j}$ the element at i^{th} line and j^{th} column of Π.
Denote by a and k one of the three axes in the fixed frame $\mathcal{R}^f$, $a \in \{x, y, z\}$ and $k \in \{0, 1, 2\}$ refer respectively to the longitudinal, lateral and vertical dimensions.

hal-00675527, version 1 - 1 Mar 2012

The control can then be chosen as:

$$\begin{aligned} v_a \quad = -\sigma_{N_a}\Big(&\Pi_{a_{3,3}} p_{3k+3} + \sigma_{\gamma_2(\Pi_{a_{3,3}} p_{3k+3}, L_{a_3}, M_{a_2})} \\ &(\Pi_{a_{2,3}} p_{3k+3} \Pi_{a_{2,2}} p_{3k+2} + \dots \\ &\sigma_{\gamma_1(\Pi_{a_{2,3}} p_{3k+3} + \Pi_{a_{2,2}} p_{3k+2}, L_{a_2}, M_{a_1})} \\ &(\Pi_{a_{1,3}} p_{3k+3} + \Pi_{a_{1,2}} p_{3k+2} + \Pi_{a_{1,1}} p_{3k+1}))\Big) \end{aligned} \tag{17}$$

For the longitudinal movement, the subscript a defines the x axis and $k = 0$. N_x $(a = x)$ is the saturation bound of the control along the $\vec{x}^f$ axis, σ and γ are respectively the saturation and level functions defined by (4) and (5).

The asymptotic stability of (p_1, p_2, p_3) is proved using [18, 31].

4.3.2. Stabilization of the lateral and vertical movements (p_5, p_6, p_8, p_9)

System (16) associates the lateral movement to the vertical and roll movements of the FMAV as for PVTOLs (Planar Vertical Taking Off and Landing) aircrafts [32, 33]. η_1 is considered as an intermediate input for system (16) and should track a desired angle η_{1_d}:

$$\eta_{1_d} = \arctan(\frac{-v_y}{v_z + 1})$$

v_y and v_z will be determined later on.
The vertical normalized lift v_h is given by:

$$v_h = \sqrt{v_y^2 + (v_z + 1)^2}$$

When the roll angle η_1 tends towards the desired value η_{1_d}, system (16) will be transformed into the form of two independent third order integrators [33]:

$$\left\{ \begin{array}{lcl} \dot{p_4} & = & p_5 \\ \dot{p_5} & = & p_6 \\ \dot{p_6} & = & v_y \end{array} \right. \qquad \left\{ \begin{array}{lcl} \dot{p_7} & = & p_8 \\ \dot{p_8} & = & p_9 \\ \dot{p_9} & = & v_z \end{array} \right.$$

Therefore, the stability of the lateral and vertical movements can be ensured using the control law (17) with $a = y$ and $k = 1$ for the y axis, $a = z$ and $k = 2$ for the z axis.

N_y and N_z are the saturation bounds of the control laws, they are chosen such that:

$$N_h = \sqrt{N_y^2 + (N_z + 1)^2} \tag{18}$$

hal-00675527, version 1 - 1 Mar 2012

with N_h the saturation bound of v_h.

The asymptotic stability of $(p_4, \ldots, p_9)$ is then ensured using [18, 31, 33].

Finally, the desired roll angle η_{1_d} defines a desired orientation of the body (the desired pitch and yaw angles are 0): $q_d = [\cos\frac{\eta_{1_d}}{2} \ \sin\frac{\eta_{1_d}}{2} \ 0 \ 0]$. The quaternion error is defined by:

$$q_e = q \ \otimes \ q_d^{-1}$$

where q^{-1} is the quaternion conjugate of q given by $q^{-1} = [q_0 \ - \ q_v^T]^T$, $\otimes$ is the quaternion product defined by $q \ \otimes \ Q = [(q_0 Q_0 - \ q_v^T Q_v) \ \ (q_0 Q_v + \ Q_0 q_v + \ q_v \times \ Q_v)^T]^T$, and $\times$ denotes the cross product. The desired angular velocity can then be computed:

$$[0, \omega_d] = 2\dot{q}_d \ \otimes \ q_d^{-1} \Rightarrow \omega_d = [\dot{\eta}_{1_d} \ 0 \ 0]$$

with

$$\dot{\eta}_{1_d} = \frac{-\dot{v}_y(v_z + 1) + v_y \dot{v}_z}{v_y^2 + (v_z + 1)^2}$$

v_y and v_z are defined by (17), $\dot{v}_y$ and $\dot{v}_z$ can be obtained by deriving analytically v_y and v_z. The analytical expression of $\dot{v}_y$ and $\dot{v}_z$ are omitted in the present paper for sake of simplicity; interested readers can refer to [34] for more details.

The angular velocity error is given by: $\omega_e = \bar{\omega} - \omega_d$. Applying the control law defined in (14) on the error dynamics, the convergence of the attitude, lateral and vertical movements is ensured.

4.3.3. Stability of the translational movement of the time varying system

Applying the proposed control law, $(\bar{P}^f - \ P_d) \rightarrow \ 0$ and $(\bar{V}^f - V_d) \rightarrow 0$. By means of the averaging theory, $\|P^f \ - \ \bar{P}^f\| < k_3 T$ and $\|V^f - \bar{V}^f\| < k_4 T$ for $k_{3,4} > 0$ and T the wingbeat period.

5. Application

5.1. Closed loop block diagram

In spite of the progress in technology, no prototype has executed so far an autonomous flight. The smallest prototype that exists [15] is still not capable of autonomous flight but only of vertical movement while guided by wires [17, 35], the energy is supplied using an external cable. On the other hand,

hal-00675527, version 1 - 1 Mar 2012

scientists are not able to explain and quantify all unsteady aerodynamic effects present at low Reynolds numbers characterizing flapping insects. Consequently, an evolutionary simulator of flapping flight is not quite achieved yet. Moreover, the constricting weight of FMAVs necessitates, among other constraints, that embedded control laws be very simple. Therefore, a simplified model is proposed in the present work in order to compute the three dimensional control laws. The simplification will be validated through some robustness tests in the next section.

The block diagram representing the flapping flight is shown in Figure 3 where each block is detailed thereafter.

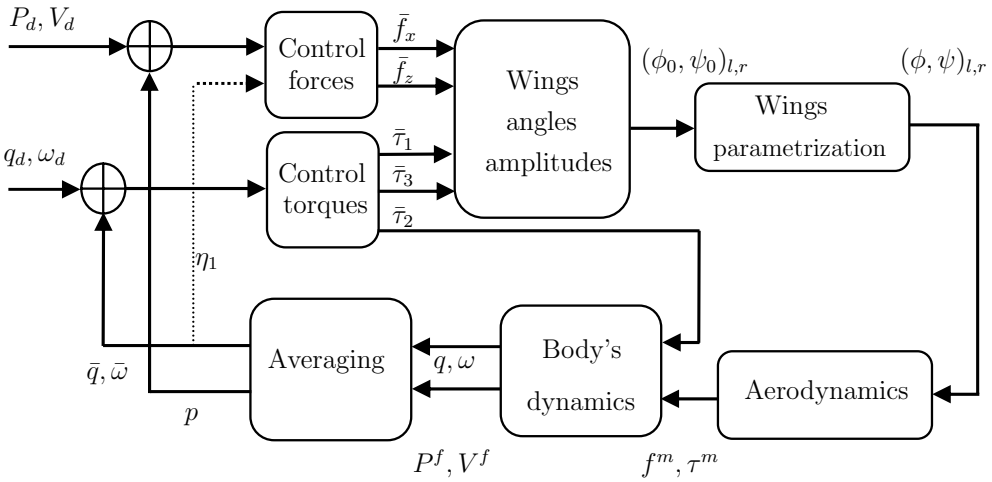

Figure 3: Block diagram of the flapping flight

Wings parametrization. In the present model, each wing is considered as a rigid body beating in the mean stroke plane in order to use actuators for two degrees of freedom only, as mentioned previously. Flapping and rotation angles, ϕ and ψ, are assumed to vary according to saw tooth and pulse functions respectively, such that the wing changes its orientation at the end of each half stroke. This should not be understood as the real movement of the wings but as the objective for a local control law of the wings.

Remark 2. *It should be emphasized here that, with most of the actuators developed in microelectronics (which all have fast dynamics) and in particular with piezoelectric actuators, the time response can reach the microsecond range. The actuator's influence on the overall dynamics of the wings is*

hal-00675527, version 1 - 1 Mar 2012

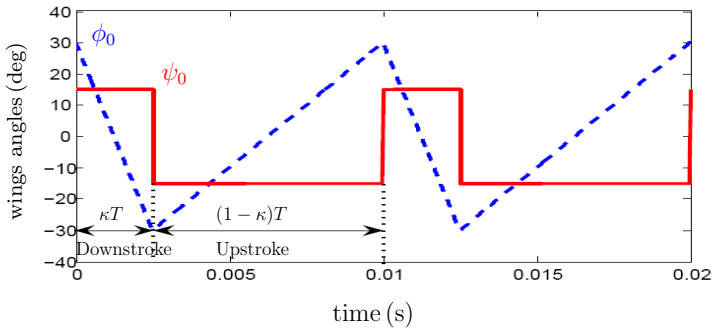

Figure 4: Wings angles over two wingbeat periods: flapping angle ϕ (dashed line) and rotation angle ψ (continuous line).

therefore of minor effect. Moreover, since the aerodynamic force affects the movements of FMAV only by its average over a wingbeat period, the influence of the actuator will be rather rendered minor. Consequently, the peculiar influence of the actuator is not visible on the FMAV's motion. This will be emphasized with some simulations in the next section.

The temporal variation of the wings trajectory is given by:

$$\begin{array}{rcll} \phi(t) & = & \left\{ \begin{array}{l} \phi_0(1-\frac{2t}{\kappa T}) \\ \phi_0(2\frac{t-\kappa T}{(1-\kappa)T}-1) \end{array} \right. & \begin{array}{l} 0 \le t \le \kappa T \\ \kappa T < t \le T \end{array} \\ \psi(t) & = & \psi_0 \text{sign}(\kappa T - t) & 0 \le t \le T \\ \theta(t) & = & 0 & 0 \le t \le T \end{array} \tag{19}$$

where sign designates the classical sign function (2), $T = 0.01\,s$ is the wingbeat period, ϕ_0 and ψ_0 are respectively the amplitudes of flapping and rotation angles and $\kappa = 0.25$ is the ratio of downstroke duration to the wingbeat period chosen arbitrarily such that $0 < \kappa < 0.5$ in order to accelerate the wing during downstroke and create an aerodynamic lift that balances the FMAV's weight. ϕ_0 and ψ_0, considered for both left and right wings, will be taken as control inputs as explained before.

Aerodynamics. Different mechanisms act cooperatively to produce the aerodynamic force in flapping flight [36, 37]: quasi-steady aerodynamics, rotational circulation, added mass, wake capture, delayed stall, etc. The first one is developed during the translational movement of the wing (the flapping movement), while the others are generated due to the rotation of the wing. The aerodynamic forces are considered perpendicular to the wing surface through its center which is located at the quarter distance of the wing's

hal-00675527, version 1 - 1 Mar 2012

center chord C_h from the leading edge ($l_t = \frac{1}{4}C_h$) and at $0.6 - 0.7$ of the wing's length L measured from the base ($l_r = 0.65L$) [38, 14] (the indexes (r, t) refer respectively to the radial (spanwise) and tangential directions of the wing).

The quasi-steady force has the opposite direction of the wing's velocity. Its module is considered proportional to the square of the wing's velocity relative to $\mathcal{R}^m$. The wings inertial forces have an indirect effect on the aerodynamic forces. This effect is small because the mass of the insect's wings is less than 5% of the body's mass [38] and is admittedly beyond the scope of this paper. The module f_{qs} of the quasi-steady aerodynamic force is given by:

$$f_{qs} = -\frac{1}{2}\rho C_w S_w v^w |v^w| \tag{20}$$

ρ is the air density, S_w is the wing's surface, v^w is the wing's velocity, C_w is a coefficient of the aerodynamic force applied on a wing. $C_w = C(1 + C_f)$ during downstroke and $C_w = C(1 - C_f)$ during upstroke, where $C \approx 3.5$ is the force coefficient derived empirically in [36], [38] and C_f is a coefficient chosen so that the aerodynamic force is 20% greater during downstroke than during upstroke. This dissymmetry between the two half-strokes can be justified based on [2]. During downstroke, the dorsal side of the wing is opposite to the air flow. The supination opposes the ventral side of the wing to the flow. Consequently, the effective area of the wing is reduced and the orientation of the air circulation about the wing reverses, leading to a wing camber alteration. Therefore, downstroke lift is likely to be higher than that of upstroke, so that the averaged force over a single wingbeat period should at least balance the body's weight.

The wing rotating about its span-wise axis, during pronation or supination, causes the air around to deviate. As a reaction to this phenomenon, the wing generates additional rotational circulation [37]. This force can be modeled as [25]:

$$f_r = \pi \rho l_r C_h^2 (\frac{3}{4} - \frac{l_t}{C_h}) v^w \dot{\psi} \tag{21}$$

with $\dot{\psi}$ is the first derivative of the rotation angle.

The added mass phenomenon is due to the additional fluid mass acceleration developed around the wing when it accelerates and rotates. It can be modeled by [25]:

$$f_m = \frac{\pi}{4}\rho L l_r C_h^2 \ddot{\phi} \tag{22}$$

hal-00675527, version 1 - 1 Mar 2012

with $\ddot{\phi}$ is the second derivative of the flapping angle.

The aerodynamic force developed by a wing and expressed in the wing's frame $\mathcal{R}^w$ is given by:

$$f^w = f_{qs} + f_r + f_m \tag{23}$$

Projecting the left and right wings aerodynamic forces into frame $\mathcal{R}^m$ ($R^m_{l,r}$ are the rotation matrices from $\mathcal{R}^w_{l,r}$ to $\mathcal{R}^m$) and summing them, the global aerodynamic force is obtained:

$$f^m = R^m_l \ f^w_l + R^m_r \ f^w_r$$

Within the chosen wings parametrization, the aerodynamic force has two components: the thrust that ensures a longitudinal forward movement of the FMAV, and the lift that ensures a vertical one.

In the sequel, the radial axis of a wing frame is taken at the quarter distance from the leading edge, i.e. the radial axis passes through the wing's aerodynamic center. The position of the wing's center, relative to $\mathcal{R}^w$ and $\mathcal{R}^m$ respectively, is:

$$\begin{aligned} p^w &= [l_r \ 0 \ 0]^T \\ p^m &= R^m_w p^w \end{aligned}$$

l_r is as defined before. The wing's velocity relative to $\mathcal{R}^m$ is obtained by deriving the position p^m, and is expressed in $\mathcal{R}^w$ by applying an appropriate rotation ($R^w_m = R^{m\,-1}_w = R^{m\,T}_w$):

$$\begin{aligned} v^m &= \dot{p}^m \\ v^w &= R^w_m v^m \end{aligned}$$

Remark 3. *Note that the relative velocity due to vortices is not considered in this work. A work on fish modeling shows that the effect, on the overall motion, of this phenomenon as well as the nonlinear dynamic phenomenon, characteristic of small Reynolds numbers, can be shrewdly taken into account with a modification of the masses and parameters of the system [39].*

Finally, the aerodynamic torque relative to $\mathcal{R}^m$ is defined as the cross product of the force f^m and the wing's aerodynamic center position. Angular viscous torques are negligible with respect to aerodynamic torques [38].

$$\tau^m(t) = p^m_l(t) \times f^m_l(t) + p^m_r(t) \times f^m_r(t) \tag{24}$$

hal-00675527, version 1 - 1 Mar 2012

Body's dynamics. The block "Body's dynamics" computes the linear and angular positions and velocities of the FMAV given the forces and torques applied to the body. Equations and computational details are given in §3.2.

Averaging. In this block, the average states over a wingbeat period are computed.

Control torques. The control torque (14) is computed based on the rotational error dynamics in order to stabilize the orientation and angular velocity of the FMAV (cf. §4.2).

Control forces. The control forces (17), with $a \in \{x, y, z\}$ and $k \in \{0, 1, 2\}$, are computed based on coupling between the vertical and roll movements aiming to stabilize the position and linear velocity of the FMAV (cf. §4.3).

Wing angle amplitudes. As explained before, the wings are parameterized using only the flapping and rotation angles. The thrust and lift, besides the roll and yaw torques are generated due to the flapping and rotating wings. Therefore, computing the averaged dynamics of the system, "Λ" in (13) is defined by a trigonometric function of its arguments, it has the following explicit form:

$$\begin{aligned} \bar{f}_x &= -\alpha\Big[\phi_0^r \sin\phi_0^r \sin\psi_0^r + \phi_0^l \sin\phi_0^l \sin\psi_0^l\Big] \\ \bar{f}_z &= \beta\Big[\phi_0^r \sin\phi_0^r \cos\psi_0^r + \phi_0^l \sin\phi_0^l \cos\psi_0^l\Big] \\ \bar{\tau}_1 &= \beta l_r\Big[{\phi_0^r}^2 \cos\psi_0^r - {\phi_0^l}^2 \cos\psi_0^l\Big] \\ \bar{\tau}_3 &= \alpha l_r\Big[{\phi_0^r}^2 \sin\psi_0^r - {\phi_0^l}^2 \sin\psi_0^l\Big] \end{aligned} \tag{25}$$

with

$$\begin{aligned} \alpha &= \tfrac{2}{T^2}\tfrac{1+(1-2\kappa)C_f}{\kappa(1-\kappa)}\rho C S_w l_r^2 \\ \beta &= \tfrac{2}{T^2}\tfrac{1-2\kappa+C_f}{\kappa(1-\kappa)}\rho C S_w l_r^2 \end{aligned}$$

Consequently, $(\phi_0^l, \phi_0^r, \psi_0^l, \psi_0^r) = \Lambda^{-1}(\bar{f}_x, \bar{f}_z, \bar{\tau}_1, \bar{\tau}_3)$ with $\bar{f}_x, \bar{f}_z, \bar{\tau}_1, \bar{\tau}_3$ are the control forces and torques respectively (cf. §4.3, 4.2).

Note that within the wings parametrization (19), only the quasi-steady aerodynamic force (20) is taken into account in the averaged forces and torques computation; the forces generated by the rotational circulation (21) and added masses (22) are null because $\ddot{\phi} = \dot{\psi} = 0$.

hal-00675527, version 1 - 1 Mar 2012

5.2. Control constraints

The control forces and torques should be bounded in order to avoid the saturation of the actuators driving the flapping wings. Considering that:

$$\begin{array}{rcccl} 0 & \leq & \phi_0 & \leq & \phi_{0_{max}} \\ 0 & \leq & \psi_0 & \leq & \psi_{0_{max}} \end{array} \tag{26}$$

for left and right wings, system (25) defines a convex set Ω in the control variables ($\bar{f}_x,\ \bar{f}_z,\ \bar{\tau}_1,\ \bar{\tau}_3$) (Figures 6(a) and 6(b), $\Omega_{\bar{\tau}_1,\bar{\tau}_3}$ and $\Omega_{\bar{f}_x,\bar{f}_z}$ are the projection of Ω on the planes $(\bar{\tau}_1,\bar{\tau}_3)$ and $(\bar{f}_x,\bar{f}_z)$ respectively). Therefore, anywhere in the set Ω, there exists a wing configuration ($\phi_0^l,\ \phi_0^r,\ \psi_0^l,\ \psi_0^r$) producing the mean desired forces and torques $(\bar{f}_x,\bar{f}_z,\bar{\tau}_1,\bar{\tau}_3)$.

6. Simulations and robustness tests

"Diptera" insect [2] is the model adopted for simulations. It has a mass of $200\,mg$ and a wingbeat frequency of $100\,Hz$. Its maximum flapping angle amplitude is $\phi_{0_{max}} = 60\,^\circ$. The wing is supposed to rotate up to $\psi_{0_{max}} = 90\,^\circ$ about its span-wise axis. The wingspan and wings surface are assumed respectively to $2L = 3\,cm$ and $2S_w = 1.14\,cm^2$, so that a vertical ascendant movement can be achieved using flapping angle amplitudes lower than the maximum value. Note that the progress in micro technology affords nowadays components having very low size and weight. For example, the structure of the OVMI prototype, developed by the project's partners, is about $40\,mg$ including an actuator (Figure 5). Concerning the on-board electronics, one can mention the circuit developed within the project weighing $100\,mg$ and composed of a microprocessor, inertial and optic flow sensors. Low weight and size sensors exist also on the market as the MPU-6000 of InvenSense which is composed of three rate gyros, tri-axis accelerometer and a microprocessor weighing less than $100\,mg$ in a package of $4\times4\times0.9\,mm$. The only equipment that can not be embarked currently is the battery, the system's power is considered ensured through a cable.

Using these numerical values, admissible sets for control forces $\Omega_{\bar{f}_x,\bar{f}_z}$ and torques $\Omega_{\bar{\tau}_1,\bar{\tau}_3}$ can be determined (25).
$\Omega_{\bar{\tau}_1,\bar{\tau}_3}$ has been approximated to the largest ellipse E_r that fits inside $\Omega_{\bar{\tau}_1,\bar{\tau}_3}$ (Figure 6(a)) for computation simplification reasons. Therefore, the control torques $\bar{\tau}_1$ and $\bar{\tau}_3$ should respect an ellipsoidal admissible set defined by:

$$[\bar{\tau}_1\ \bar{\tau}_3]Q_1[\bar{\tau}_1\ \bar{\tau}_3]^T \leq 1 \tag{27}$$

hal-00675527, version 1 - 1 Mar 2012

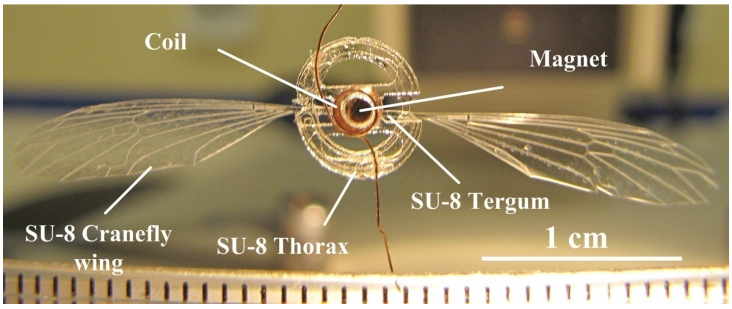

Figure 5: The OVMI prototype developed by the project partners.

where Q_1 is a diagonal definite positive matrix representing the ellipse's semi-axes. Practically, if $\bar{\tau}_1 \geq M_{2,1}$ (14), $\bar{\tau}_1$ could be saturated to $M_{2,1}$, consequently $\bar{\tau}_3$ will be equal to zero. To avoid a null yaw control torque in this case, 70% of $M_{2,1}$ will be attributed to $\bar{\tau}_1$, $\bar{\tau}_3$ will be calculated by (27) defining then a set Ω_r (Figure 6(a)). This choice is justified by the necessity to bring the FMAV to the horizontal plane first.
The admissible set of thrust and lift forces $\Omega_{\bar{f}_x,\bar{f}_z}$ is drawn in Figure 6(b). It is approximated to the largest semi-ellipse E_t that fits inside (E_t almost coincides with $\Omega_{\bar{f}_x,\bar{f}_z}$). It is defined by:

$$\begin{array}{rcl} [\bar{f}_x \ \bar{f}_z] Q_2 [\bar{f}_x \ \bar{f}_z]^T & \leq & 1 \\ \bar{f}_z & \geq & 0 \end{array} \tag{28}$$

where Q_2 is a diagonal definite positive matrix representing the semi-ellipse's semi-axes. A fixed saturation level mgN_h inside E_t is attributed to $\bar{f}_z$ since it will be decomposed in mgN_y and mgN_z (18) (for computation simplification reasons). The saturation bound is calculated such that more power is given to the lateral movement because it is associated to the roll movement (99% of E_t's vertical semi-axis is attributed to mgN_h): the FMAV can then be brought to the horizontal plane rapidly. The saturation bound mgN_x of the thrust $\bar{f}_x$ satisfies the semi-ellipse's equation (28).

The proposed control law is tested through some simulations and robustness tests.

The control is supposed to drive the FMAV from an initial position of $(1, 1, -1)$ meters and orientation of $(-40, -25, 50)$ degrees to the equilibrium defined by $(0, 0, 0)$ meters and $(0, 0, 0)$ degrees. The initial linear and angular velocities are null. The FMAV is stabilized in hovering mode at the desired position. The parameters of the control torques are set to

hal-00675527, version 1 - 1 Mar 2012

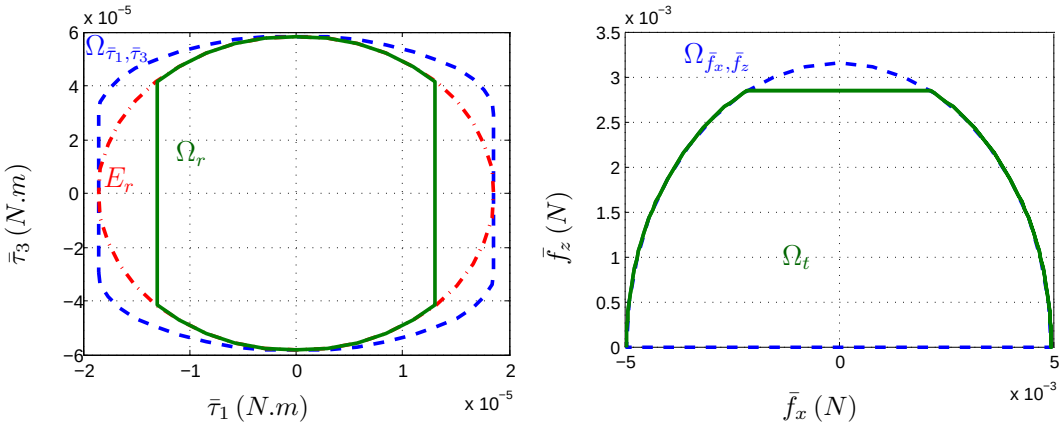

(a) Rotational saturation set (b) Translational saturation set

Figure 6: Yaw torque versus roll torque (left), defining the saturation set $\Omega_{\bar{\tau}_1,\bar{\tau}_3}$ approximated to an ellipse E_r then to a set Ω_r. Lift versus thrust (right), defining the saturation set $\Omega_{\bar{f}_x,\bar{f}_z}$ approximated to an ellipse E_t, that almost coincides with $\Omega_{\bar{f}_x,\bar{f}_z}$, then to the set Ω_t.

$\rho = (0.2, 2, 0.2)$, $\delta = (0.01, 0.1, 0.01)$ and $\lambda_i = \frac{M_{2,i}}{3.1}$. The poles placements are set to $(-3, -3, -3)$, $(-3.5, -3.5, -3.5)$ and $(-2.5, -2.5, -2.5)$ for the longitudinal, lateral and vertical movements respectively.

Figures 7 and 8 show respectively the convergence of the body's position and orientation. The position presents a high overshoot due to the choice of the control parameters. This choice has been done such that the control law ensures stability despite rude conditions of disturbances and errors in modeling and aerodynamic parameters as shown in the following. Note that once the prototype is ready for use, the model parameters will be determined accurately based on measurements or estimation strategies. Consequently, the control parameters will be set such that the control ensures an optimal movement (without high overshoot). The corresponding control forces and torques are plotted in Figures 7 and 9 respectively. Although the angular velocities seem very high, they are comparable to those observed in true insects and to the simulation results of [10]. This is due to the low inertia and the high beating frequency of insects. The desired attitude is reached in a suitable time for practical implementation and is comparable to the nature. One should also notice the saturation of the control forces, which means that the system get maximal benefit of the admissible set of control forces. This ensures a boundedness of the wing angle amplitudes (Figure 10) avoiding the

hal-00675527, version 1 - 1 Mar 2012

actuators saturation and consequently, the nonlinearities that can be engendered. At stability, the rotation angles are null stopping any longitudinal movement, the flapping angles reach a value that generates an aerodynamic force which, averaged over a wingbeat period, balances the FMAV's weight. Note also that the overshoot is not detectable during trajectory tracking, except in the beginning of the trajectory as shown in Figure 11.

The simplifications considered in the model, relative to the presence of actuators at the wings bases besides the unsteady aerodynamic forces, are validated through simulations.

Regarding the absence of prototype, some robustness tests are proposed allowing to be projected into real conditions. Such situations can reflect some imperfections of construction, identification errors, varying aerodynamic properties, disturbances due to wind, etc. Concerning the last case, when a disturbance is applied to the FMAV taking it away from the equilibrium state, the control will act to get it back to stability because the control laws proposed in this work ensure the almost global stability of the body. On the other hand, the robustness tests presented thereafter can be proved based on the perturbation theory [22]. Depending on the perturbation ε' affecting the aerodynamic coefficient, the force or the aerodynamic center, the aerodynamic force varies with respect to $\{\varepsilon', \varepsilon', \varepsilon'^2\}$ and the aerodynamic torque with respect to $\{\varepsilon', \varepsilon', \varepsilon'^3\}$ respectively. The system (6-9) can be written as:

$$\dot{x} = f(x, t, \varepsilon'^n) = f(x, t, \varepsilon) \tag{29}$$

with $n \in \{1, 2, 3\}$ and $\varepsilon = \varepsilon'^n$ is the perturbation that affects a certain parameter, principally the force and consequently the torque in the simulated examples.

The following conditions are ensured:

1. f as defined in (29) and its partial derivatives with respect to (x, ε) up to order N are continuous in (t, x, ε) for $(t, x, \varepsilon) \in [t_0, t_0 + T] \times D \times [-\varepsilon_0, \varepsilon_0]$, with $D = [\mathbb{R}^3, \mathbb{R}^3, \mathbb{H}, \mathbb{R}^3]$, and T the wingbeat period;
2. the Taylor series development of (29) at the initial state $\eta(\varepsilon) = x(t_0)$ and its derivatives up to order N are continuous for $\varepsilon \in [-\varepsilon_0, \varepsilon_0]$;
3. the nominal system obtained by setting ε to zero has a unique solution $x_0(t) \in D$ on the interval $[t_0, t_0 + T]$.

Then, there exists $\varepsilon^* > 0$ such that $\forall\ |\varepsilon| < \varepsilon^*$, (29) has a unique solution $x(t, \varepsilon)$ defined on $[t_0, t_0+T]$, which satisfies $x(t, \varepsilon) - \sum_{k=0}^{N-1} x_k \varepsilon^k = \mathcal{O}(\varepsilon^N)$.

hal-00675527, version 1 - 1 Mar 2012

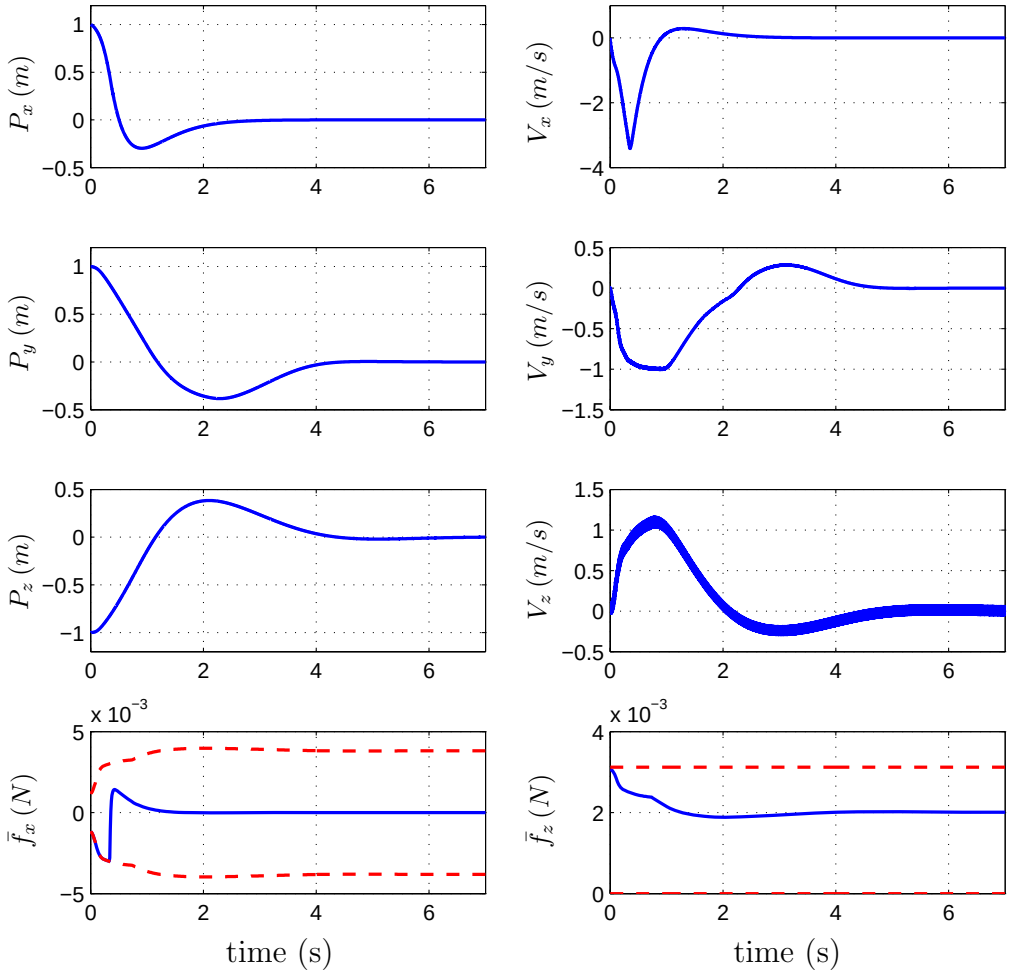

Figure 7: The linear movement of the FMAV along the 3 axes in $\mathcal{R}^f$ from initial position $(1, 1, -1)$ (left) and the corresponding linear velocities (right). The thrust and lift control forces (in $\mathcal{R}^m$) (bottom) with the saturation bounds (dashed lines): the saturation bound of $\bar{f}_x$ depends on the value of $\bar{f}_z$.

hal-00675527, version 1 - 1 Mar 2012

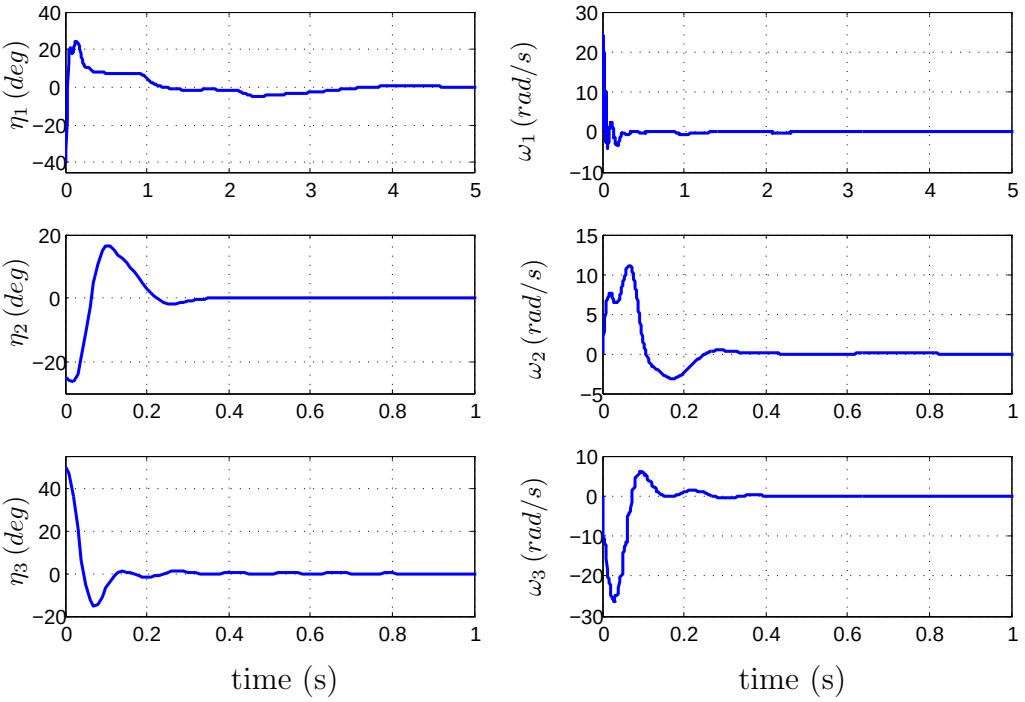

Figure 8: The convergence of the roll, pitch and yaw angles from initial orientation $(-40, -25, 50)\,^\circ$ (left) and the corresponding angular velocities (right) zoomed to the first $5\,s$ for the roll movement since it is linked to the linear displacement and to the $1^{st}\,s$ for the pitch and yaw movements.

hal-00675527, version 1 - 1 Mar 2012

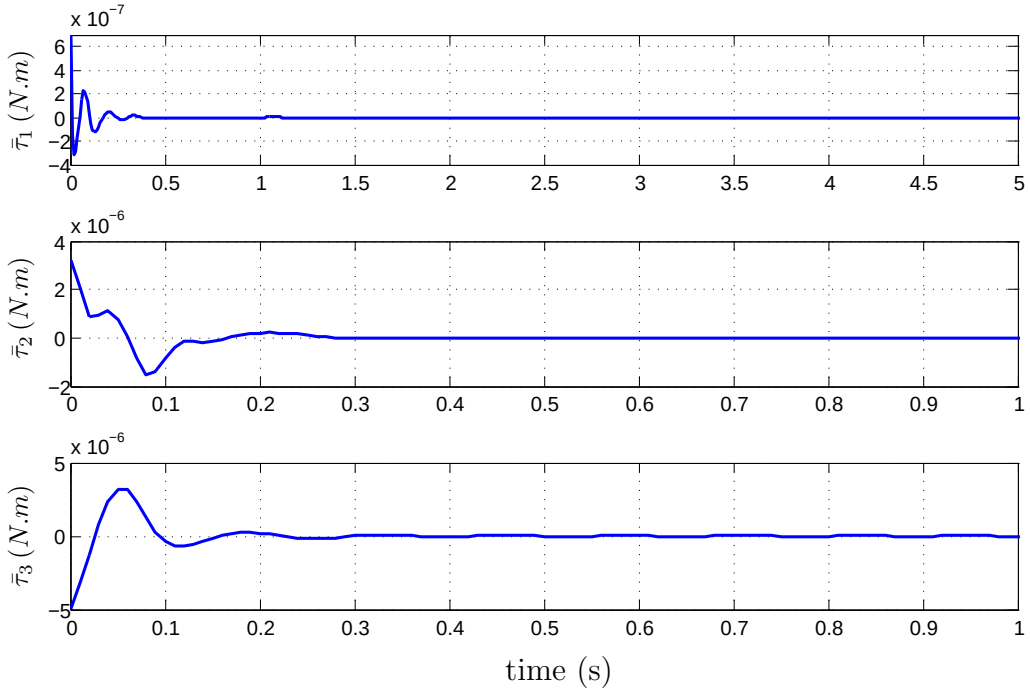

Figure 9: The roll, pitch and yaw control torques zoomed to the first $5\,s$ for the roll and the $1^{st}\,s$ for the pitch and yaw.

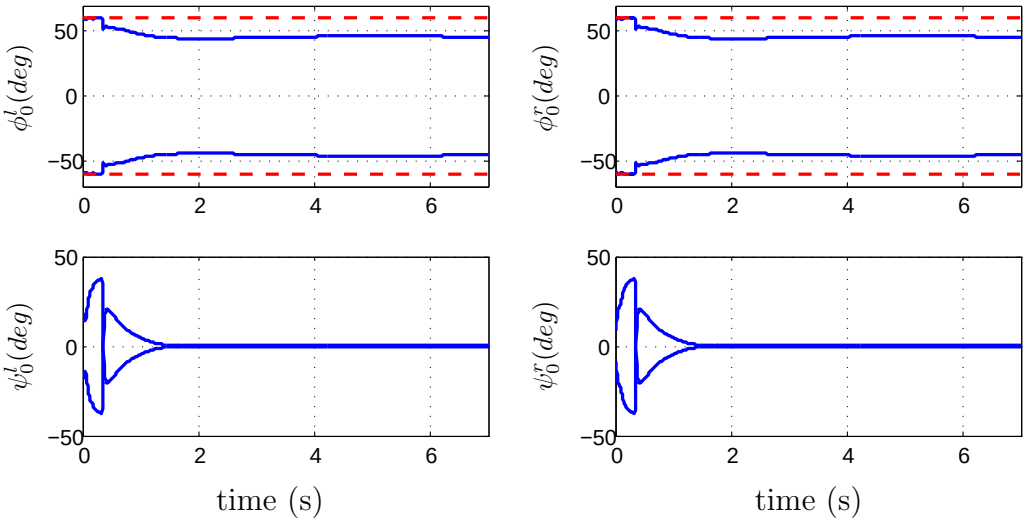

Figure 10: The wings angles amplitudes for left and right wings: the amplitudes of the flapping angles (continuous blue line) are bounded at $\phi_{0_{max}} = 60\,^\circ$ (dashed red line).

hal-00675527, version 1 - 1 Mar 2012

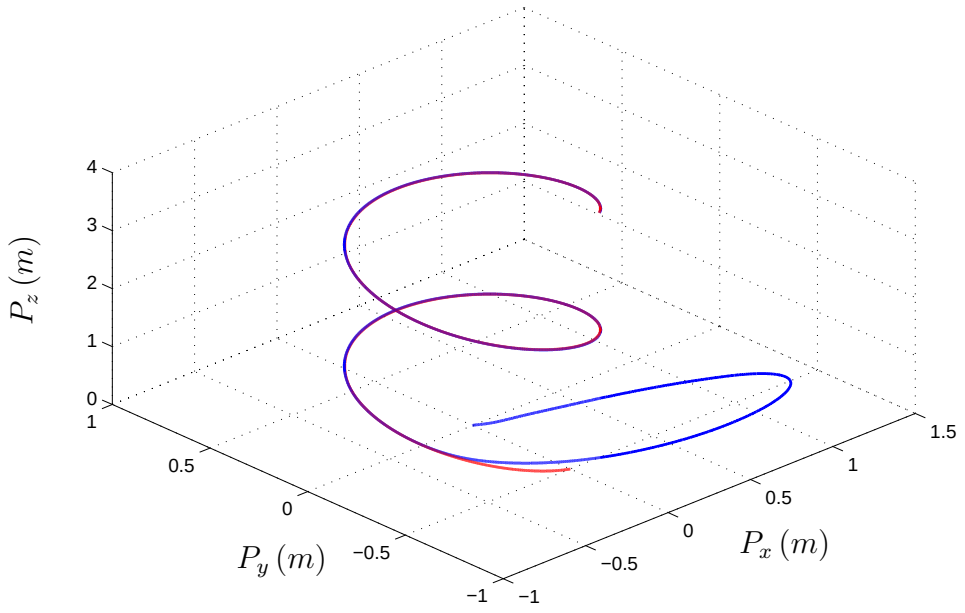

Figure 11: Trajectory tracking: The 3D trajectory of the FMAV, the desired trajectory is plotted in red and the current one in blue.

hal-00675527, version 1 - 1 Mar 2012

Considering the case where $N = 1$, then $\|x(t,\varepsilon) - x_0(t)\| \leq k\varepsilon,\ \forall|\varepsilon| < \varepsilon^*,\ \forall t \in [t_0, t_0 + T], k > 0$. $k\varepsilon$ can be interpreted as a static error between the perturbed and nominal systems solutions. The presence of the integrator in the control law (cf. §4) helps eliminating this static error and ensures stability at the equilibrium point consequently. Note that the quantification of ε^* depends on the perturbed variable and is not evident to compute analytically specially for such complex systems. Therefore, some simulations are presented thereafter to approve the theory.

6.1. Robustness with respect to actuator influence and unsteady aerodynamic forces

The theoretical control of the wings amplitudes, computed in §5, should be transmitted through actuators. For example, piezoelectric actuators, operating in resonant mode, can ensure the flapping movement of the wings. The alternative voltage applied to the actuators is delivered by a power electronic converter. This one should be conceived especially for piezoelectric actuators, which are reactive loads [40, 41] and present a nonlinear behavior (hysteresis, creep). The aerodynamic forces represent another important source of non linearity. Whence arises the necessity of adding a low level wing controller [13, 42], which reference signal is provided by the high level flapping flight control (Figure 4). So, in the block diagram (Figure 3), an additional block called "Actuators" (including "Piezoelectric device", "Power electronics" and "Non linear control") may be added between "Wing parametrization" and "Aerodynamics". Taking into consideration the local control of the piezoelectric actuator, the whole entity (actuator and local controller), defining the"Actuators" block, behaves as a first order filter with a response time of $0.1\,ms$ (acceptable value since a wingbeat period is of $10\,ms$ and the ratio of the downstroke duration to the wingbeat period is taken to 0.25). Note that different types of piezoceramic actuators available on the market (PZT for example) have response time ranging from milliseconds to microseconds. Figure 12 presents the input signals (reference wing angles) and output signals (real wing angles) of the "Actuators" block. Once the actuator is introduced, the first derivative of the rotation angle and the second derivative of the flapping angles are non null. Therefore, the forces, due to the rotational circulation and added mass effects, cooperate with the quasi-steady aerodynamic force to ensure the flight (23). The robustness of the computed control laws with respect to the actuator and consequently to the additional generated forces is showed in Figures 13, 14, 15, 16.

hal-00675527, version 1 - 1 Mar 2012

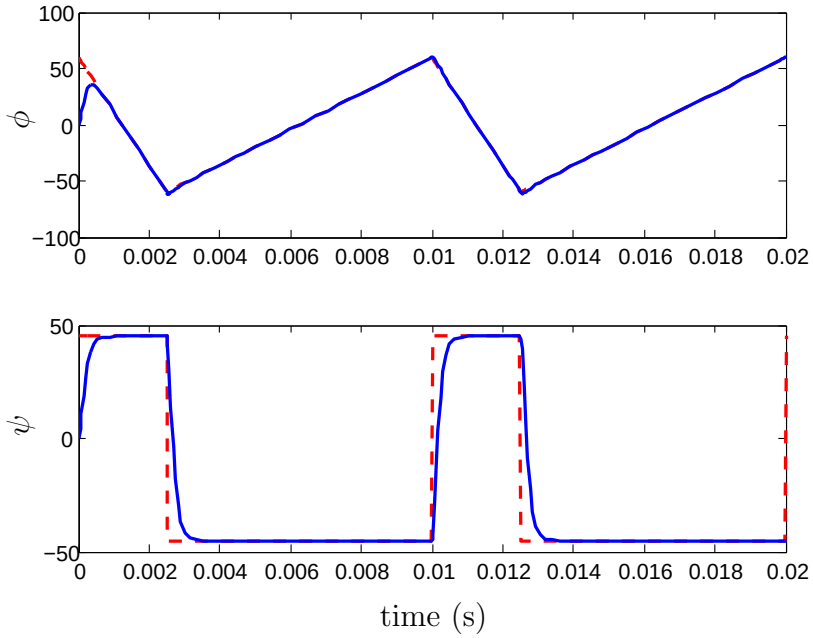

Figure 12: The flapping (top) and rotation (bottom) wing angles: the reference angles in dashed lines and the real angles in continuous line.

hal-00675527, version 1 - 1 Mar 2012

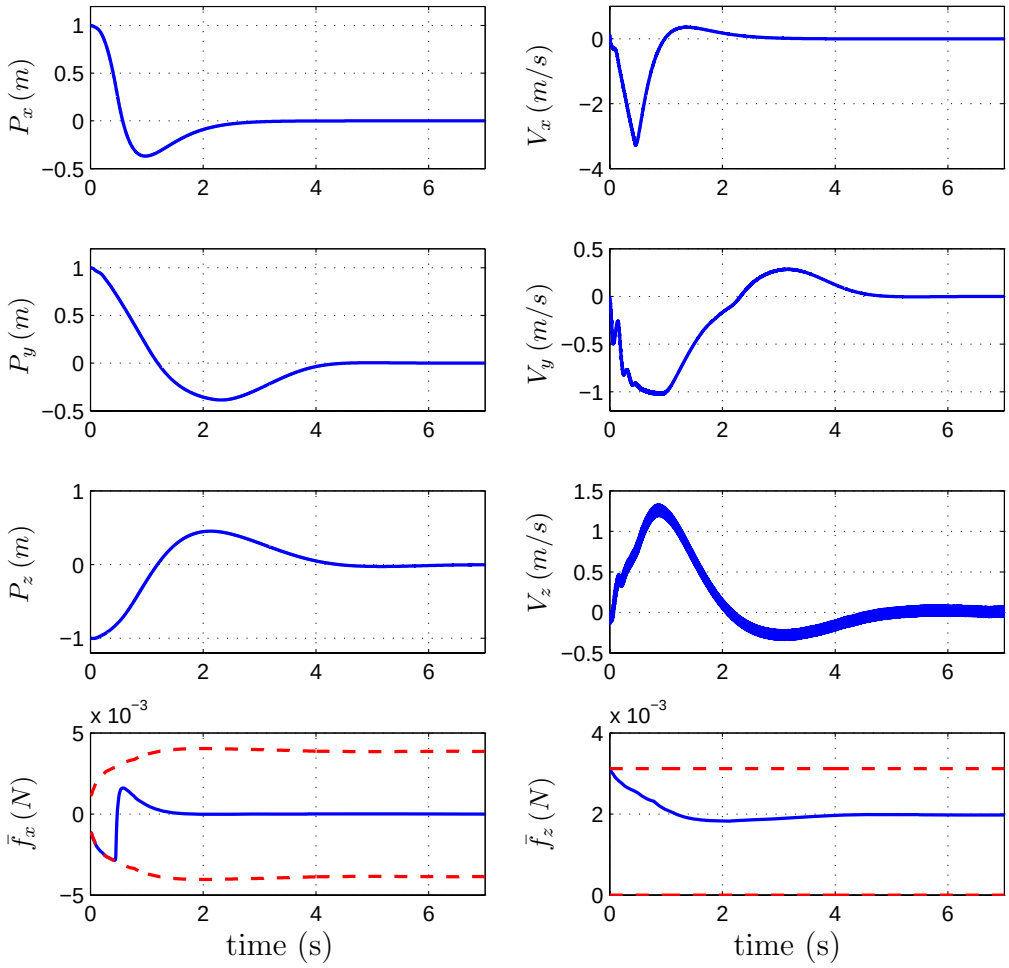

Figure 13: The convergence of the FMAV's position (left), velocity (right) and control forces (bottom) in presence of the actuator and the unsteady aerodynamic forces.

hal-00675527, version 1 - 1 Mar 2012

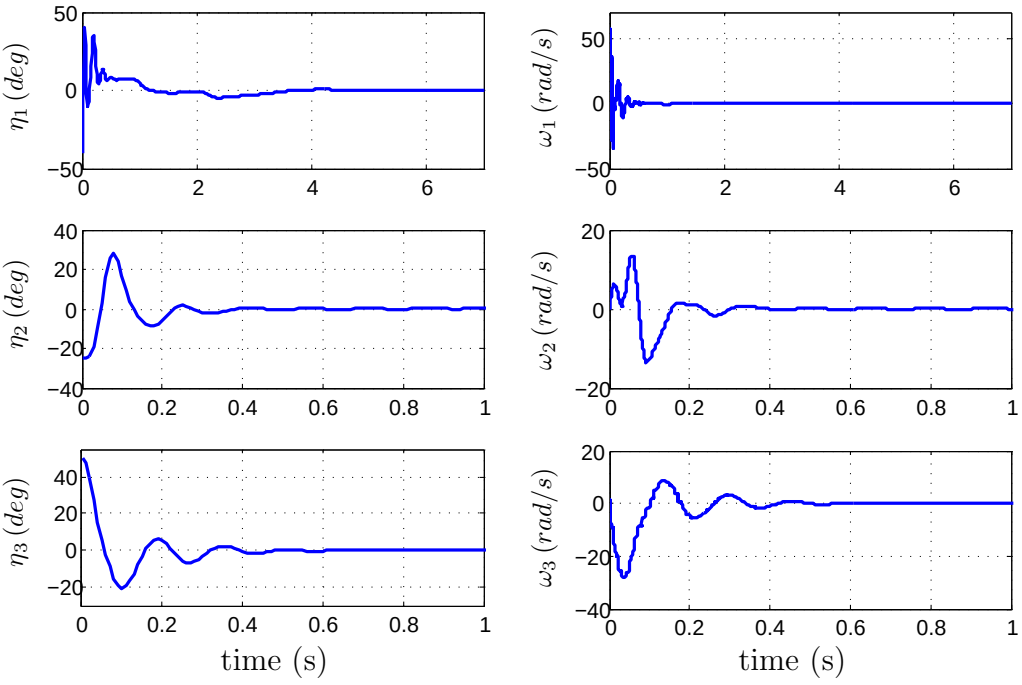

Figure 14: The convergence of the roll, pitch and yaw angles (left) and the corresponding angular velocities (right), zoomed to the 1^{st} s for pitch and yaw, in presence of the actuator and the unsteady aerodynamic forces.

hal-00675527, version 1 - 1 Mar 2012

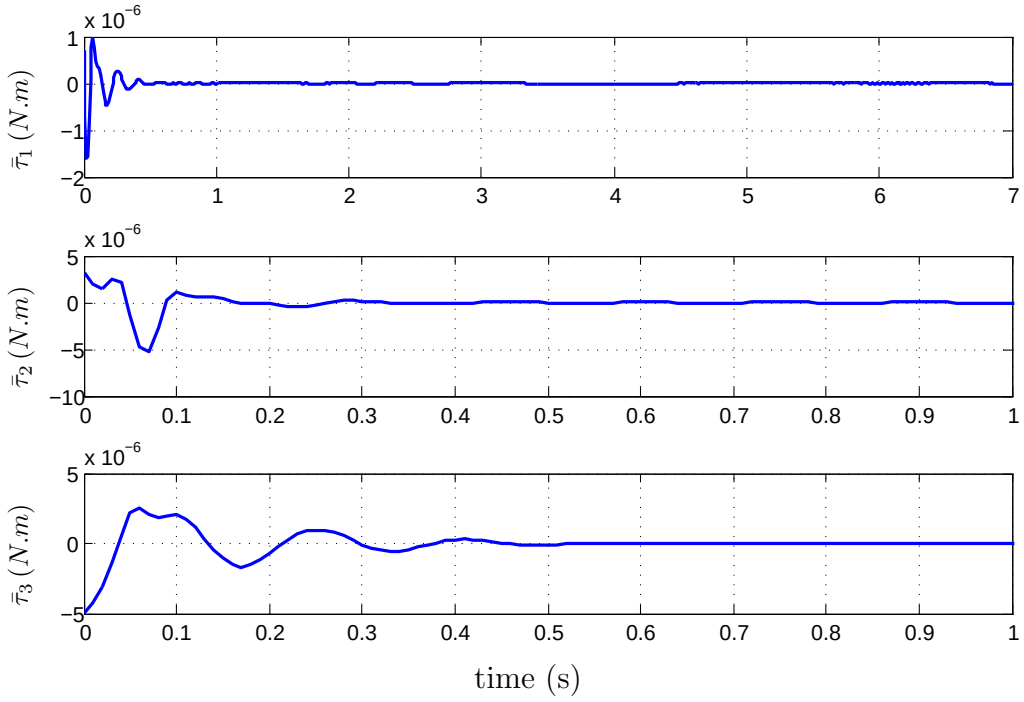

Figure 15: The roll, pitch and yaw control torques, zoomed to the first 1^{st} s for pitch and yaw, in presence of the actuator and the unsteady aerodynamic forces.

hal-00675527, version 1 - 1 Mar 2012

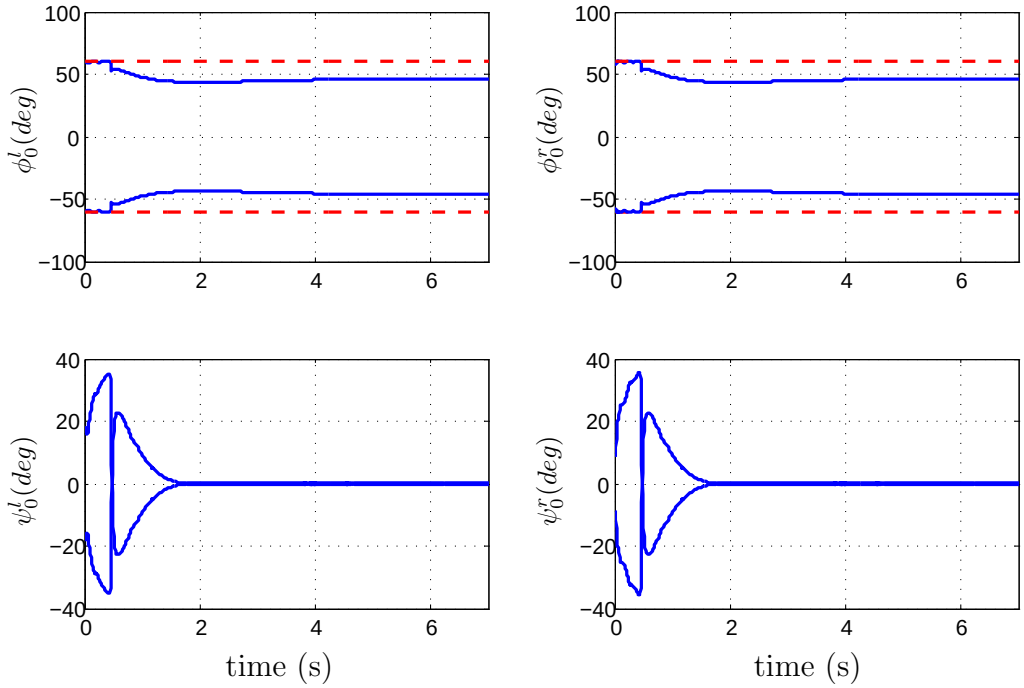

Figure 16: The wings angles amplitudes for left and right wings in presence of the actuator and the unsteady aerodynamic forces.

hal-00675527, version 1 - 1 Mar 2012

6.2. Robustness with respect to external disturbances

The external disturbances are assimilated to external forces and torques applied to the body. The FMAV has been perturbed at $t = 7\,s$ during 10 wingbeat periods. The magnitude of the disturbances, over the three axes, is $(5.10^{-3}, 5.10^{-3}, 3.10^{-3})\,N$ for the forces and $3.10^{-5}\,N.m$ for the torques, values considered in $\mathcal{R}^m$. Note that a rain drop weighs about $5.10^{-6}\,N$. Such high values of the disturbances are simulated only to show the importance of the saturations in regaining stability. One can notice the saturation of the roll and pitch torques (Figure 19) as well as the flapping angles (Figure 20). The control torques and forces cooperate in order to overcome the disturbances and ensure stability. The results of simulations are shown in Figures 17, 18, 19 and 20. The FMAV reaches very high angular velocities that risk to break the prototype under such constraints. One should emphasize that real insects can not resist to this kind of circumstances, principally because of their low inertia.

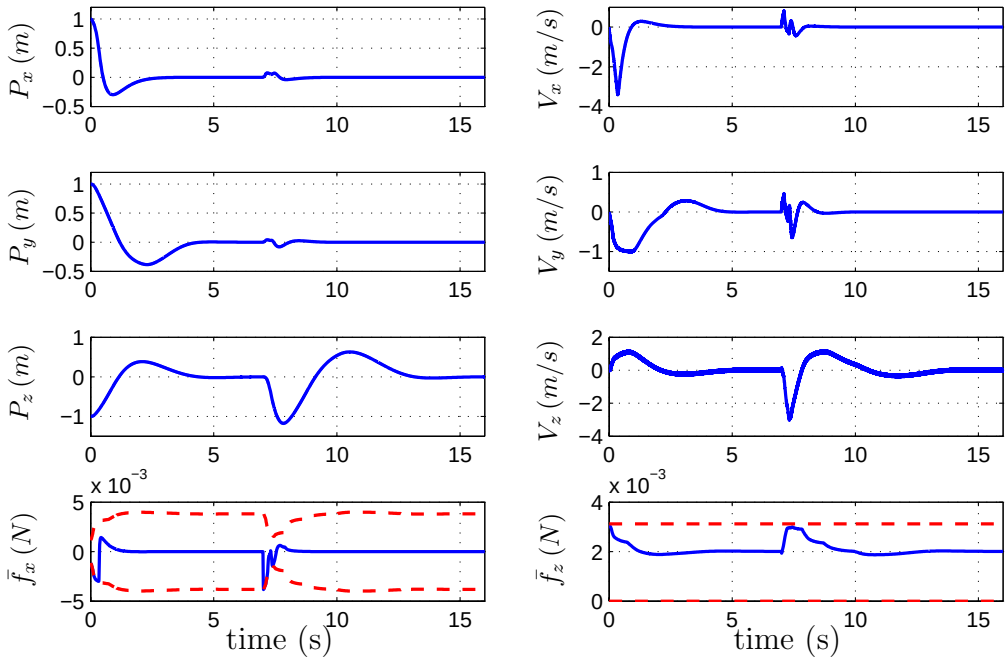

Figure 17: The linear movement of the FMAV in presence of disturbances applied at $t = 7\,s$ for the duration of 10 wingbeat periods (left) and the corresponding linear velocities (right). The thrust and lift control forces (bottom).

hal-00675527, version 1 - 1 Mar 2012

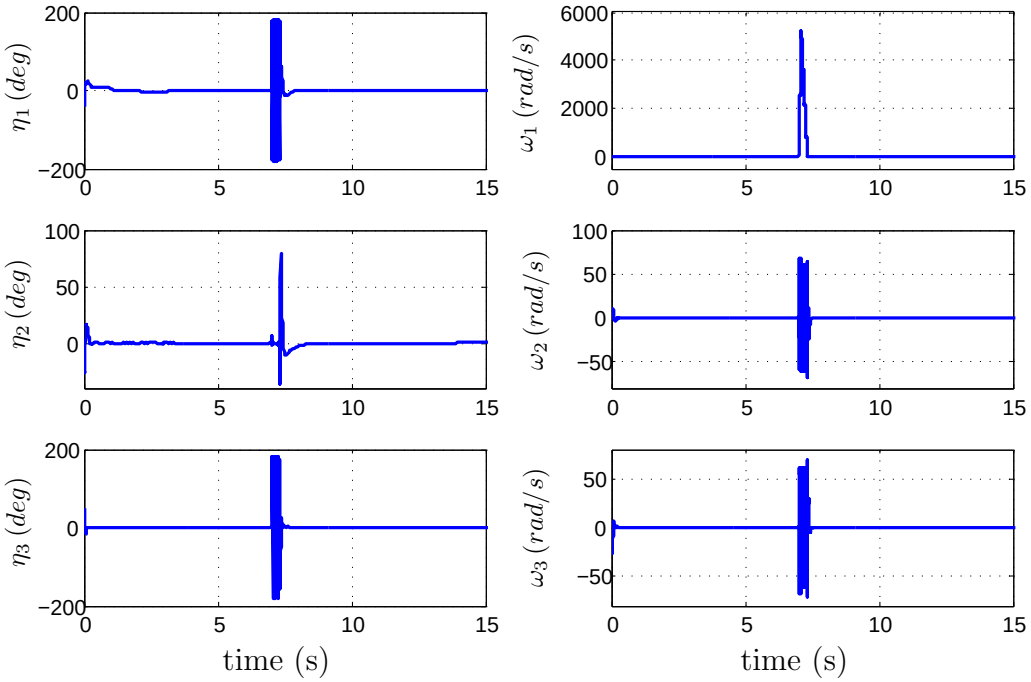

Figure 18: The convergence of the roll, pitch and yaw angles in presence of disturbances (left) and the corresponding angular velocities (right).

hal-00675527, version 1 - 1 Mar 2012

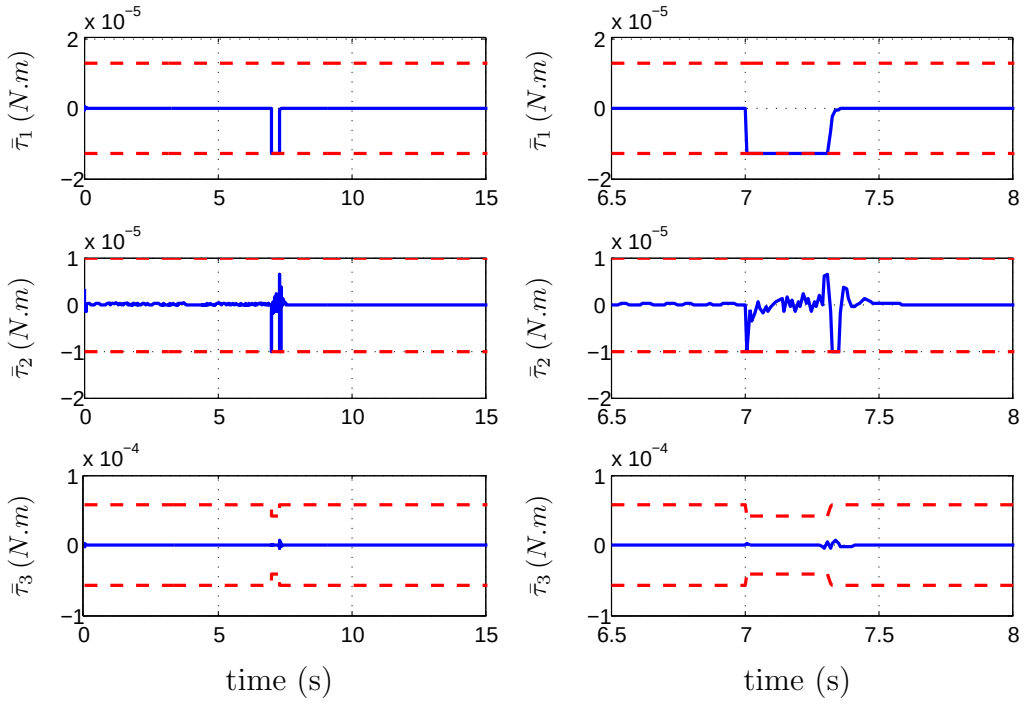

Figure 19: The roll, pitch and yaw control torques in presence of disturbances (left) zoomed to show the effect of the disturbances (right). The saturation bound of $\bar{\tau}_3$ depends on the value of $\bar{\tau}_1$.

hal-00675527, version 1 - 1 Mar 2012

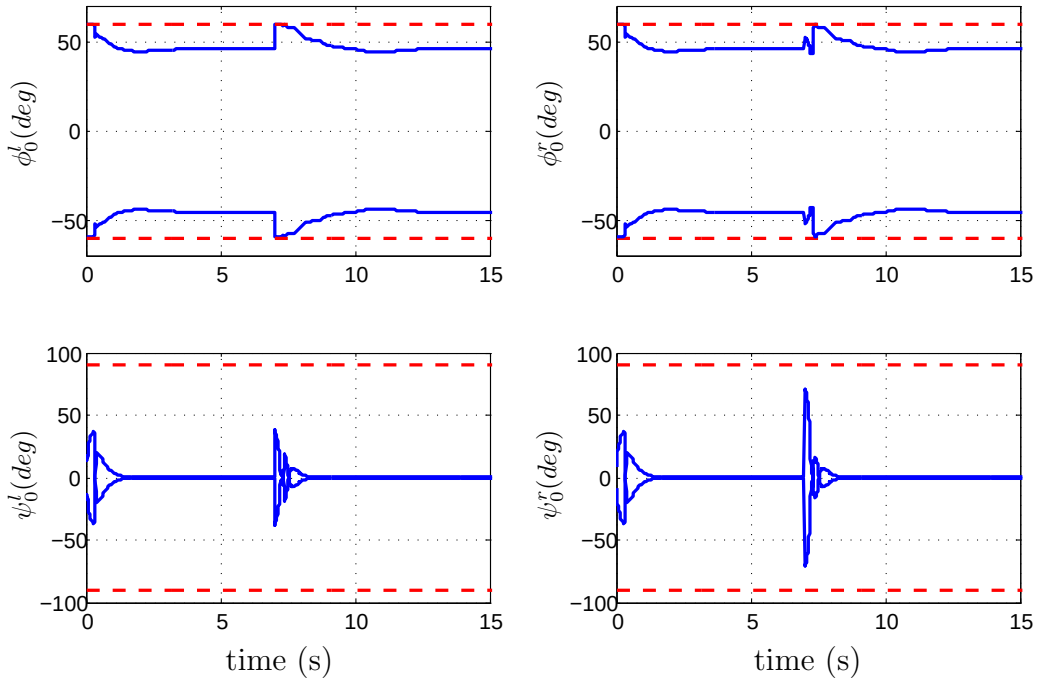

Figure 20: The wings angles amplitudes for left and right wings in presence of disturbances.

hal-00675527, version 1 - 1 Mar 2012

Note that the duration of the disturbance does not affect the convergence of the system; increasing the duration will take the FMAV much farther from the equilibrium position, while executing many rotations about its axes, which will increase the time to reach back the stability.

6.3. Robustness with respect to aerodynamic errors

The robustness of the control laws is tested for a bad estimation of the aerodynamic coefficient C, known to be difficult to identify. This property is essential for real time implementation where the aerodynamic coefficient may be poorly measured and/or the FMAV may execute missions in areas having different aerodynamic characteristics. A subtractive error is introduced to C in order to reduce its value:

$$C_{dist} = C - \Delta C$$

where ΔC is a stochastic parameter subject to a uniform distribution, such that C_{dist} varies within the interval $[2, 3.5]$. A different value of ΔC, within the uniform distribution, is applied at the beginning of each wingbeat period. Such a quick variation of C is not realistic; it is simulated only to emphasize the control law robustness shown in Figures 21, 22, 23 and 24. The aerodynamic error mainly affects the vertical movement. The stochastic aspect is detectable on the vertical linear velocity and control lift, besides the amplitudes of the flapping angles. Notice that the FMAV needs a longer time to reach stability, relative to the nominal case (Figure 7). Note also that the control lift and flapping angles are stabilized at values greater than that corresponding to FMAV's weight balance (Figure 10). This increase of the control inputs (lift, wing angles) aims to balance the decrease of the aerodynamic lift caused by the drop of the aerodynamic coefficient.

6.4. Robustness with respect to errors in the positions of the wings aerodynamic centers

The manufacture of the wings may result in some dissymmetry between the left and right wings. This imperfection in fabrication can be modeled by locating the wings centers of pressure asymmetrically. The simulations presented in this paragraph are realized with an error of $[5, 50, 0]\,\%$ for the position of the right wing center of pressure relative to the nominal position defined in §5. The considered asymmetry generates aerodynamic roll and pitch torques. Figure 25 shows the convergence of the position, linear velocity

hal-00675527, version 1 - 1 Mar 2012

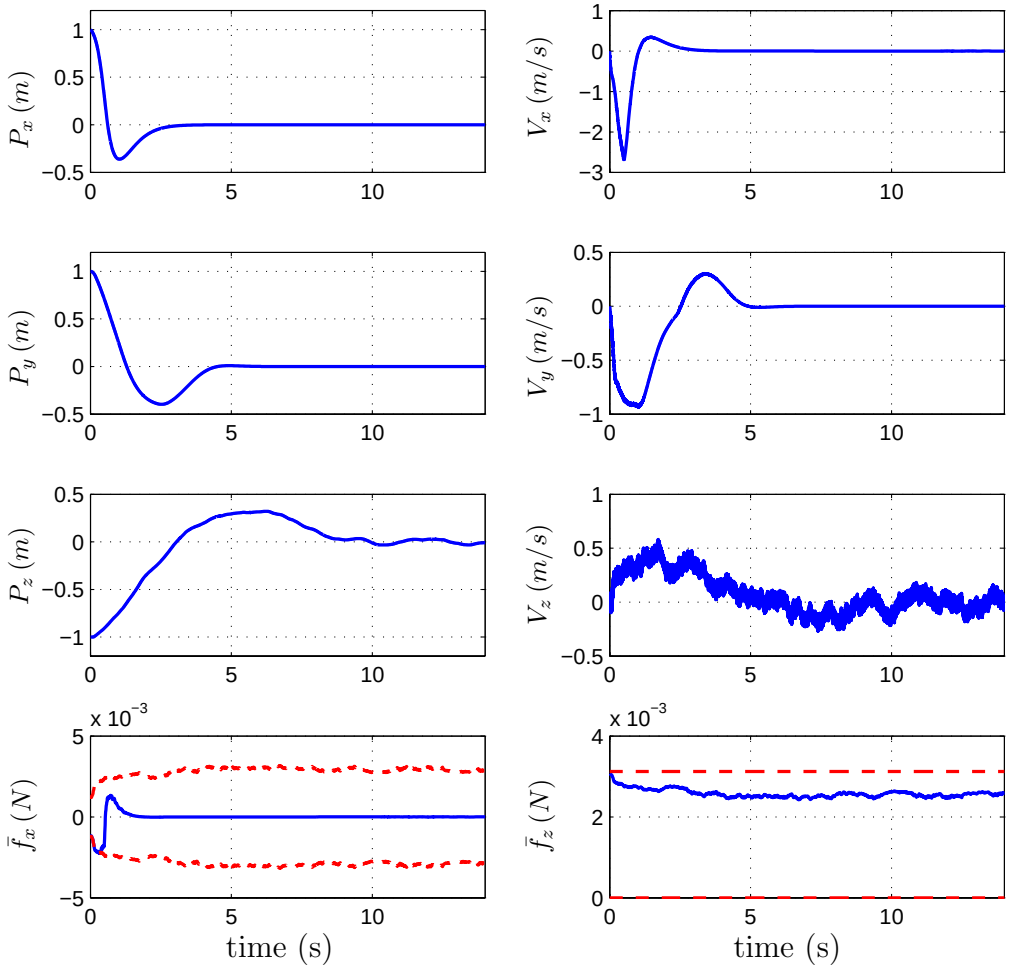

Figure 21: The convergence of the FMAV's position (left), velocity (right) and control forces (bottom) in presence of aerodynamic coefficient uncertainty.

hal-00675527, version 1 - 1 Mar 2012

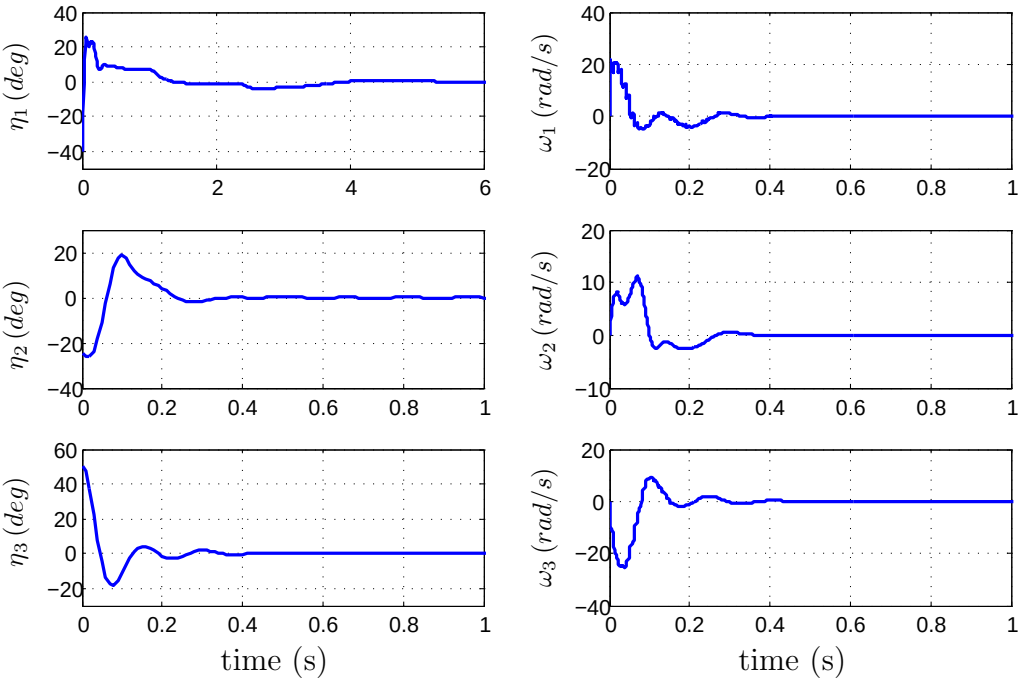

Figure 22: The convergence of the roll, pitch and yaw angles (left) and the corresponding angular velocities (right), zoomed to the first s for pitch and yaw, in presence of aerodynamic coefficient uncertainty.

hal-00675527, version 1 - 1 Mar 2012

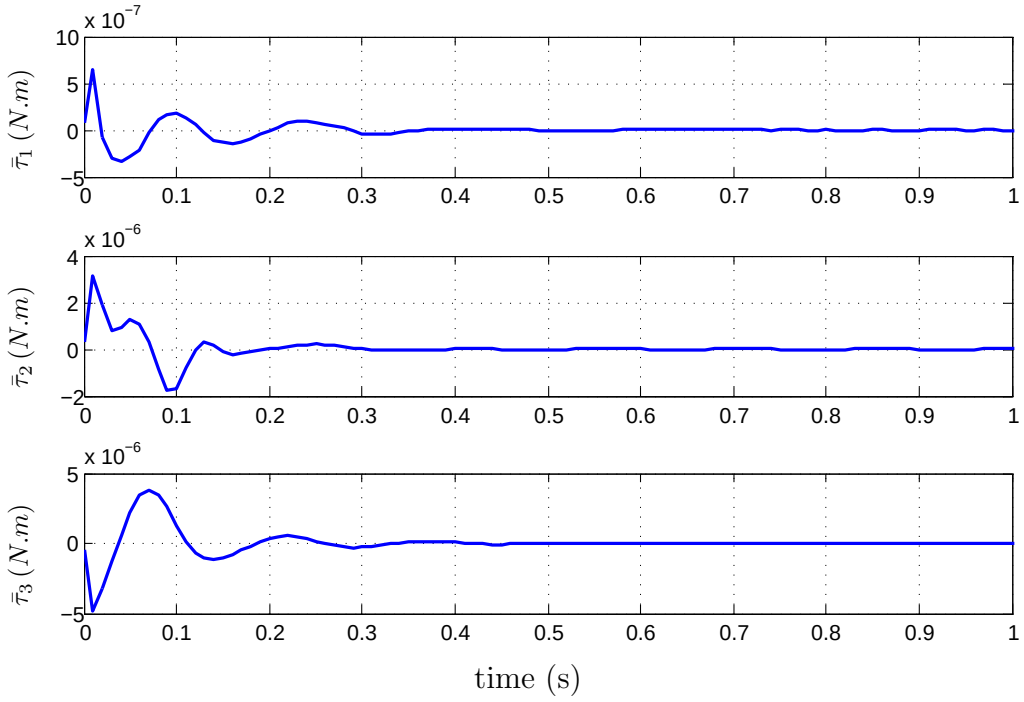

Figure 23: The roll, pitch and yaw control torques zoomed to the first s in presence of aerodynamic coefficient uncertainty.

hal-00675527, version 1 - 1 Mar 2012

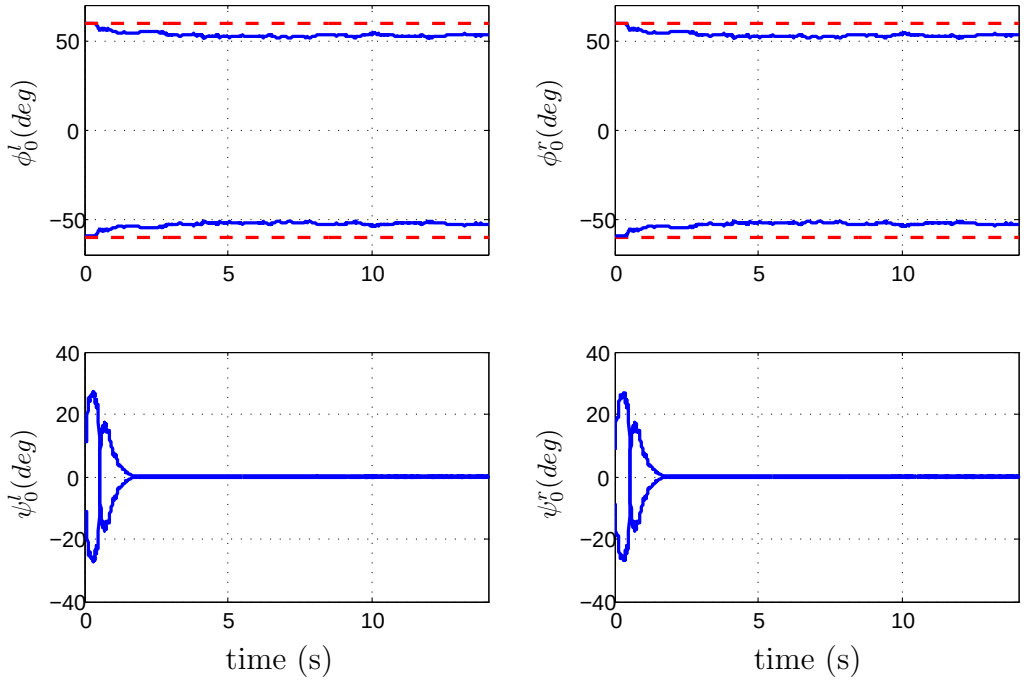

Figure 24: The wings angles amplitudes for left and right wings in presence of aerodynamic coefficient uncertainty.

hal-00675527, version 1 - 1 Mar 2012

and control forces. Figures 26 and 27 show respectively the convergence of the body's orientation, angular velocity and control torques. The roll and pitch control torques besides the control lift do not converge to zero but to a constant value in order to balance the torque generated by the dissymmetry in the wings centers of pressure. The asymmetry is also revealed at the flapping angle amplitudes for the left and right wings (Figure 28).

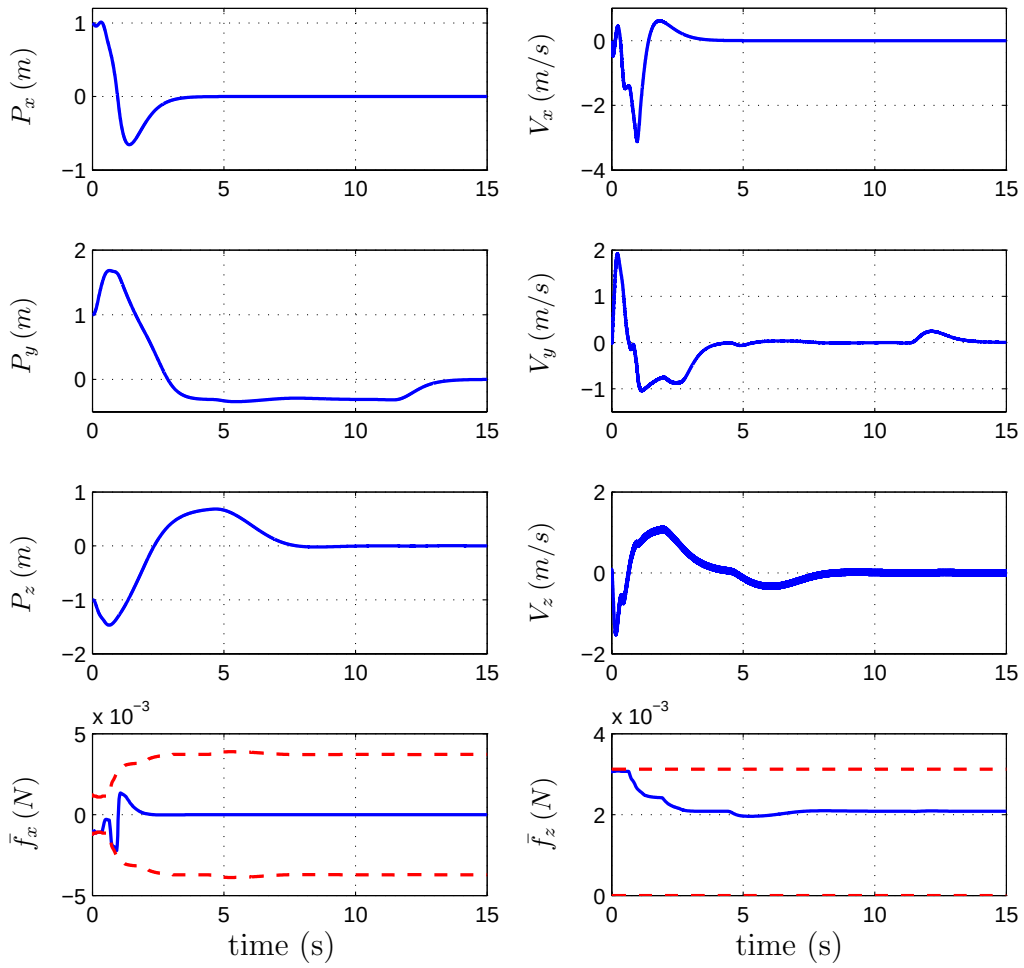

Figure 25: The convergence of the FMAV's position (left), velocity (right) and control forces (bottom) in presence of a dissymmetry in the position of the left and right wings aerodynamic centers.

hal-00675527, version 1 - 1 Mar 2012

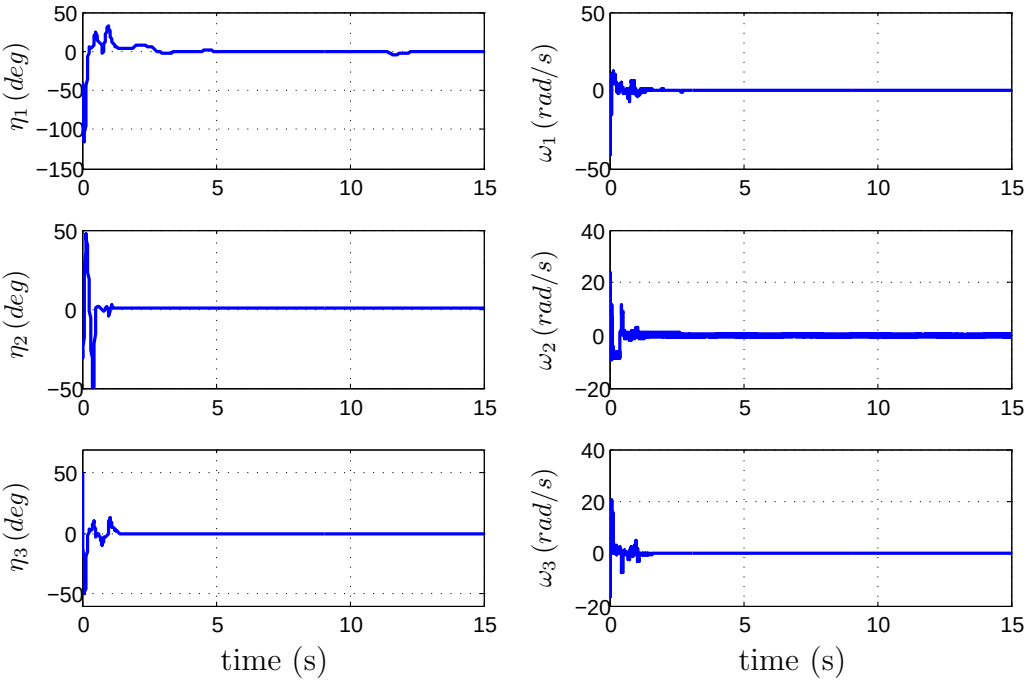

Figure 26: The convergence of the roll, pitch and yaw angles (left), and the angular velocities (right), in presence of a dissymmetry in the position of the left and right wings aerodynamic centers.

hal-00675527, version 1 - 1 Mar 2012

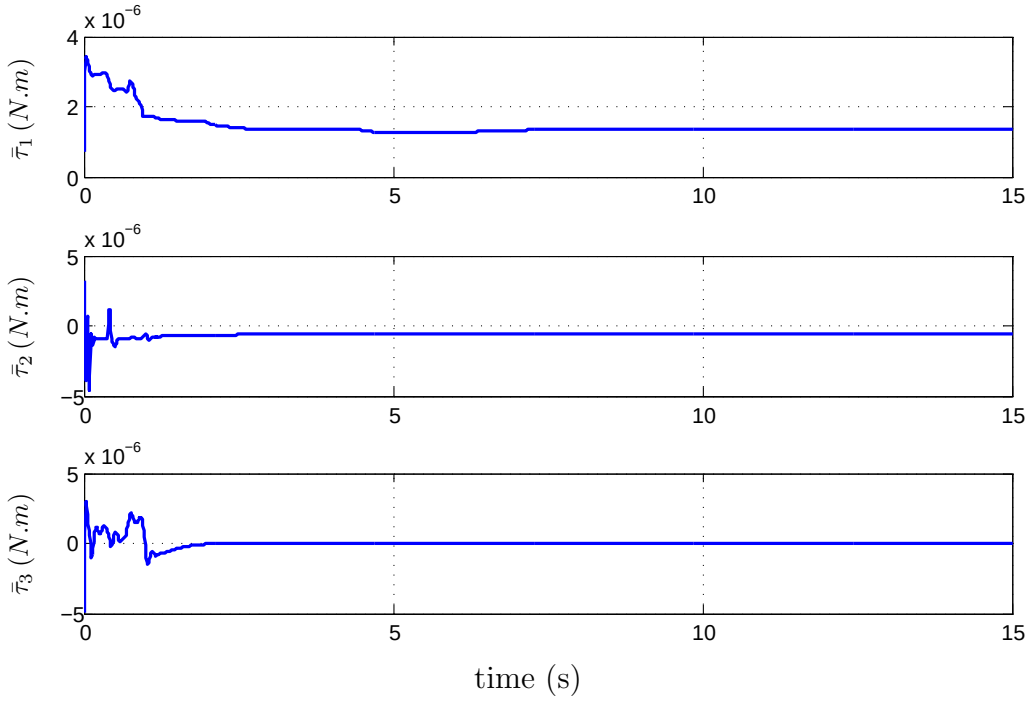

Figure 27: The roll, pitch and yaw control torques, in presence of a dissymmetry in the position of the left and right wings aerodynamic centers.

hal-00675527, version 1 - 1 Mar 2012

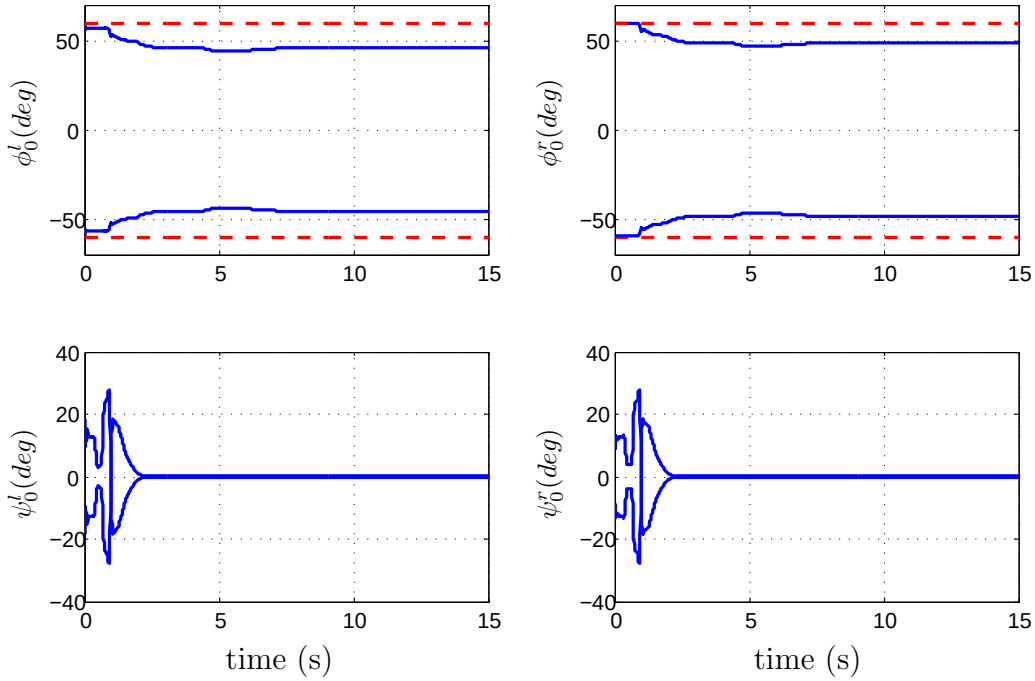

Figure 28: The wings angles amplitudes for left and right wings in presence of a dissymmetry in the position of the left and right wings aerodynamic centers.

hal-00675527, version 1 - 1 Mar 2012

6.5. Robustness with respect to a dissymmetry in the aerodynamic forces

The dissymmetry in the fabrication of the two wings may induce also a difference in the magnitude of the left and right aerodynamic forces. A ratio of 0.9 can be reached without deteriorating the FMAV's stability. The convergence of the linear and angular positions and velocities, the control forces and torques, and the wing angles are plotted in Figures 29, 30, 31 and 32. The FMAV falls at the beginning of the flight trajectory because the total aerodynamic force is reduced and can not balance the weight. The control law acts to compensate this and ensure the ascendant flight. This asymmetry creates also a roll aerodynamic torque. It follows that the roll control torque and the control lift force don't converge to zero and to the FMAV's weight respectively. Moreover, the amplitudes of the flapping angles for left and right wings are not equal (Figure 32).

7. Conclusions

A new strategy for controlling FMAVs has been presented. It is based on a bounded state feedback control of the forces and torques and takes into account the saturation of the actuators driving the flapping wings. The proposed strategy is based on the theory of cascade consisting on stabilizing the FMAV's position based on a coupling with the orientation. The controls are very simple, therefore suitable for embedded implementations. A simplified model of a FMAV, having simple wing kinematic parametrization, has been developed. The averaged model has been computed thereafter in order to determine the values of the control (wing angle amplitude) to be applied at the beginning of each wingbeat period. Different robustness tests are performed, especially with respect to model simplifications, external disturbances, modeling errors, parameters uncertainties, aiming to validate the control laws efficiency, the simplifications adopted in the model and fill in the lack of experimentations.

Future works intend to implement the proposed control laws on the prototype that is being developed in the scope of "EVA" project. The controller tuning parameters will be regulated, specifically for the prototype, such that a better performance can be guaranteed.
Being aware of the difficulty to implement estimators and/or observers in the FMAV's processor, allowing to have access to the body's states, the control laws will be managed to take directly inputs from on-board sensors measurements. These controls will also be tested on the prototype. Studies are also

hal-00675527, version 1 - 1 Mar 2012

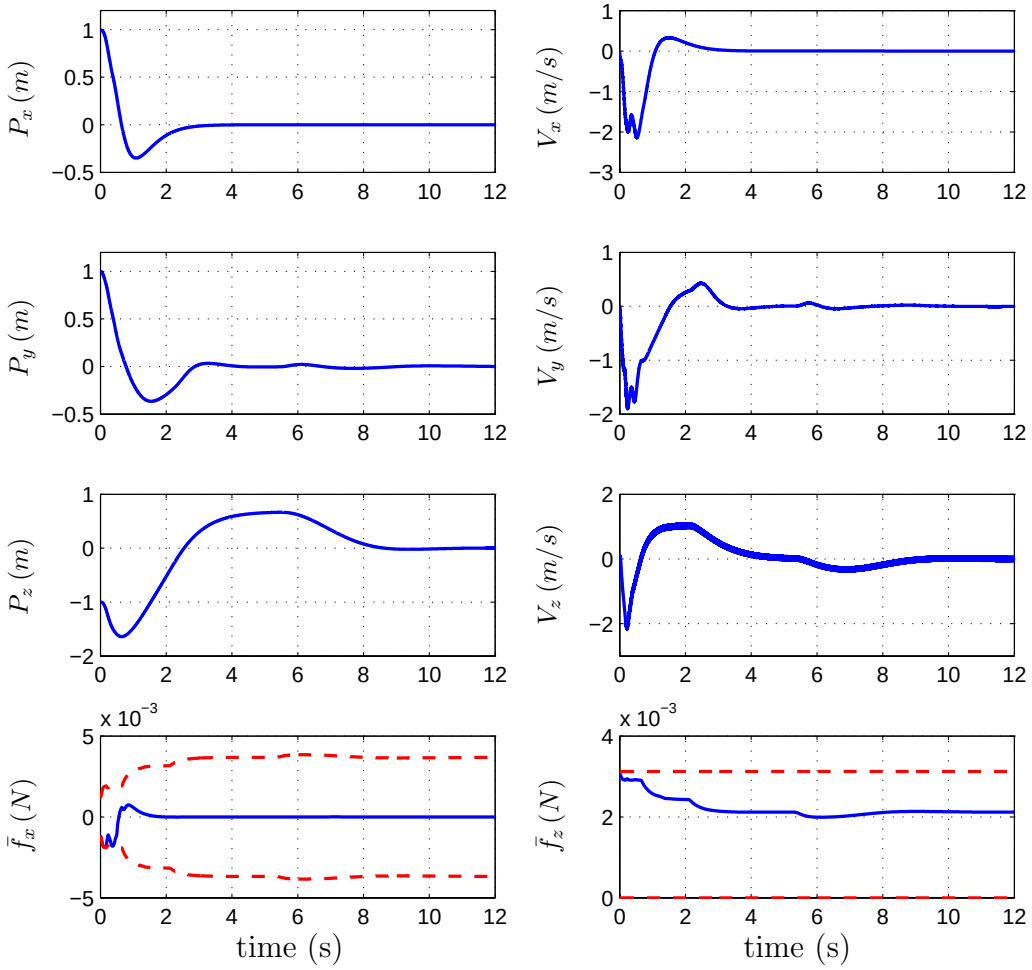

Figure 29: The convergence of the FMAV's position (left), velocity (right) and control forces (bottom) in presence of asymmetric left and right aerodynamic forces.

hal-00675527, version 1 - 1 Mar 2012

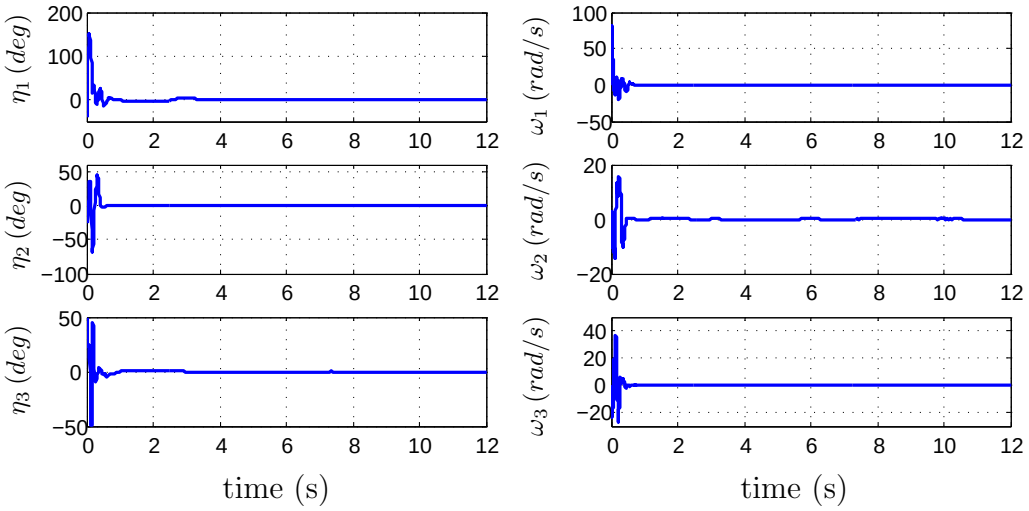

Figure 30: The convergence of the roll, pitch and yaw angles (left) and the corresponding angular velocities (right) in presence of asymmetric left and right aerodynamic forces.

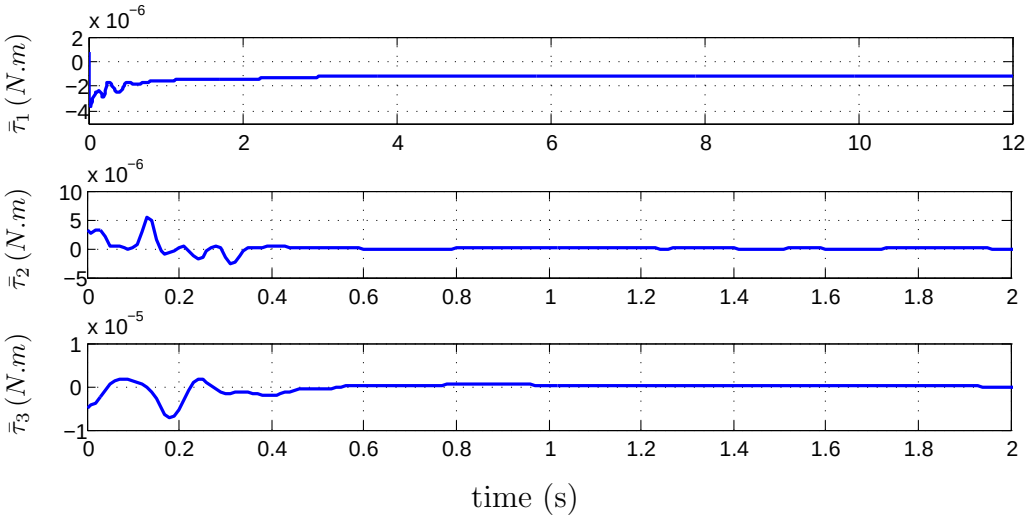

Figure 31: The roll, pitch and yaw control torques in presence of asymmetric left and right aerodynamic forces.

hal-00675527, version 1 - 1 Mar 2012

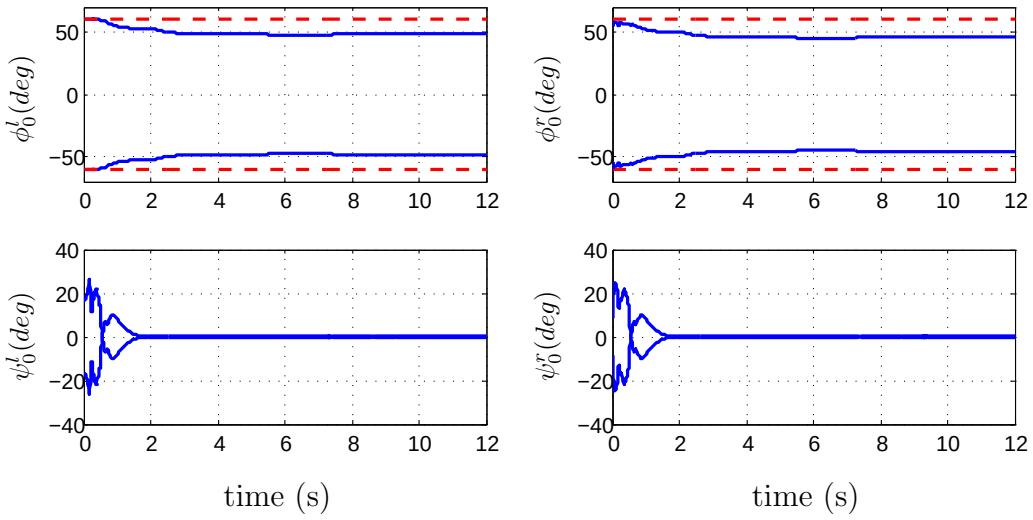

Figure 32: The wings angles amplitudes for left and right wings in presence of asymmetric left and right aerodynamic forces.

conducted to consider a passive rotation of the wings in order to reduce the number of on-board actuators and simplify the control laws.

References

[1] J. Kellogg, C. Bovais, R. Foch, Development and testing of unconventional micro air vehicle configurations, in: AIAA Unmanned Unlimited Conf., San Diego, California, 2003.

[2] R. Dudley, The biomechanics of insect flight: form, function, evolution, Princeton University Press, 2002.

[3] T. Hedrick, T. Daniel, Flight control in the hawkmoth Manduca sexta: the inverse problem of hovering, The journal of experimental Biology 209 (16) (2006) 3114–3130.

[4] X. Deng, L. Schenato, S. Sastry, Model identification and attitude control scheme for a micromechanical flying insect, in: Int. Conf. on Control, Autom., Robotic and Vision, Singapore, 2002, pp. 1007–1012.

hal-00675527, version 1 - 1 Mar 2012

[5] L. Schenato, W.-C. Wu, S. Sastry, Attitude control for a micromechanical flying insect via sensor output feedback, in: Int. Conf. on Control, Autom., Robotic and Vision, Singapore, 2002, pp. 1031–1036.

[6] L. Schenato, W.-C. Wu, S. Sastry, Attitude control for a micromechanical flying insect via sensor output feedback, IEEE Journal of Robotics and Automation 20 (1) (2004) 93–106.

[7] L. Schenato, X. Deng, S. Sastry, Hovering flight for a mocromechanical flying insect: Modeling and robust control synthesis, in: IFAC World Congress on Automatic Control, Spain, 2002.

[8] D. Campolo, G. Barbera, L. Schenato, L. Pi, X. Deng, E. Guglielmelli, Attitude stabilization of a biologically inspired robotic housefly via dynamic multimodal attitude estimation, Advanced Robotics 23 (7-8) (2009) 955–977.

[9] L. Schenato, X. Deng, S. Sastry, Flight control system for a micromechanical flying insect: Architecture and implementation, in: Int. Conf. on Robotics and Automation, Korea, 2001, pp. 1641–1646.

[10] X. Deng, L. Schenato, W.-C. Wu, S. Sastry, Flapping flight for biomimetic robotic insects: Part II- flight control design, IEEE Transactions on Robotics 22 (4) (2006) 789–803.

[11] P.-S. Sreetharan, R.-J. Wood, Passive torque regulation in an underactuated flapping wing robotic insect, Autonomous robots 31 (2-3) (2011) 225–234.

[12] S.-J. Chung, M. Dorothy, Neurobiologically inspired control of engineered flapping flight, Journal of guidance, control and dynamics 33 (2) (2010) 440–453.

[13] J. Yan, R. J. Wood, S. Avadhanula, M. Sitti, R. S. Fearing, Towards flapping wing control for a micromechanical flying insect, in: Int. Conf. on Robotics and Automation, Seoul, Korea, 2001, pp. 3901–3908.

[14] X. Deng, L. Schenato, W.-C. Wu, S. Sastry, Flapping flight for biomimetic robotic insects: Part I- system modeling, IEEE Transactions on Robotics 22 (4) (2006) 776–788.

hal-00675527, version 1 - 1 Mar 2012

[15] R. Wood, Liftoff of a 60mg flapping-wing mav, in: Proceedings of the 2007 IEEE/RSJ International Conference on Intelligent Robots and Systems, IROS'07, San Diego, CA, USA, 2007, pp. 1889–1894.

[16] B.-M. Finio, B. Eum, C. Oland, R.-J. Wood, Asymmetric flapping for a robotic fly using a hybrid power-control actuator, in: Proceedings of the 2009 IEEE/RSJ Int. Conf. on Intelligent Robots and Systems, St. Louis, MO, USA, 2009, pp. 2755–2762.

[17] N.-O. Perez-Arancibia, K.-Y. Ma, K.-C. Galloway, J.-D. Greenberg, R.-J. Wood, First controlled vertical flight of a biologically inspired microrobot, Bioinspiration and biomimetics 6 (3) (2011) 036009.

[18] N. Marchand, Further results on global stabilization for multiple integrators with bounded controls, in: IEEE Conf. on Decision and Control, CDC'2003, Hawai, USA, 2003.

[19] K. Senda, M. Sawamoto, M. Kitamura, T. Obara, K. Kanazawa Univ., Effects of flexibly torsional wings in flapping-of-wings flight of butterfly, in: World automation congress, Hawaii, USA, 2008, pp. 1–6.

[20] W. Shyy, H. Aono, S.-K. Chimakurthi, P. Trizila, C.-K. Kang, C. Cesnik, H. Liu, Recent progress in flapping wing aerodynamics and aeroelasticity, Progress in Aerospace Sciences 46 (7) (2010) 284–327.

[21] M. Shuster, A survey of attitude representations, Journal of astronautical sciences 41 (4) (1993) 439–517.

[22] H. Khalil, Nonlinear systems, Prentice Hall, 2002.

[23] F. Bullo, Averaging and vibrational control of mechanical systems, SIAM Journal on Control and Optimization 41 (2) (2002) 452–562.

[24] P. A. Vela, Averaging and control of nonlinear systems, Ph.D. thesis, California Institute of Technology (2003).

[25] T. Rakotomamonjy, T. Le Moing, M. Ouladsine, Simulation model of a flapping-wing micro air vehicle, in: European Micro Aerial Vehicle Conf., EMAV 2004, Braunschweig, Germany, 2004.

hal-00675527, version 1 - 1 Mar 2012

[26] A. Renaudin, V. Zhang, P. Tabourier, J. Camart, C. Druon, Droplet manipulation using SAW actuation for integrated microfluidics, in: μTAS, Malm, Sweden, 2004, pp. 551–553.

[27] E. Sontag, Remarks on stabilization and input-to-state stability, in: 28^{th} IEEE Conf. on Decision and Control, CDC'89, 1989.

[28] A. Isidori.

[29] J. Guerrero-Castellanos, A. Hably, N. Marchand, S. Lesecq, Bounded attitude stabilization: Application on four rotor helicopter, in: Proceedings of the 2007 IEEE Int. Conf. on Robotics and Automation, Roma, Italy, 2007.

[30] A. Teel, Global stabilization and restricted tracking for multiple integrators with bounded controls, Systems & Control Letters 18 (3) (1992) 165–171.

[31] E. N. Johnson, S. K. Kannan, Nested saturation with guaranteed real poles, in: Proceedings of the American Control Conference, Vol. 1, 2003, pp. 497–502.

[32] A. Teel, A nonlinear small gain theorem for the analysis of control systems with saturation, IEEE Transactions on Automatic Control 41 (9) (2006) 1256–1270.

[33] A. Hably, F. Kendoul, N. Marchand, P. Castillo, Further results on global stabilization of the pvtol aircraft, in: Proceedings of the Second Multidisciplinary International Symposium on Positive Systems: Theory and Applications, Grenoble, France, 2006, pp. 303–310.

[34] H. Rifai, Modelisation et commande d'un robot biomimetique volant, Ph.D. thesis, Institut Polytechnique de Grenoble (2008).

[35] R.-J. Wood, B. Finio, M. Karpelson, K. Ma, P.-S. Perez-Arancibia, N.-O. ans Sreetharan, H. Tanaka, J.-P. Whitney, Progress on "pico" air vehicles, in: International Symposium on Robotics Research, Flagstaff, AZ, USA, 2011.

[36] M. Dickinson, F.-O. Lehmann, S. Sane, Wing rotation and the aerodynamic basis of insect flight, Science 284 (5422) (1999) 1954–1960.

hal-00675527, version 1 - 1 Mar 2012

[37] S. Sane, Review The aerodynamics of insect flight, The journal of experimental Biology 206 (23) (2003) 4191–4208.

[38] L. Schenato, D. Campolo, S. Sastry, Controllability issues in flapping flight for biomimetic micro aerial vehicles (mavs), in: Int. Conf. on Decision and Control, USA, 2003.

[39] F. Boyer, M. Porez, W. Khalil, Macro-continuous computed torque algorithm for a three-dimensional eel-like robot, IEEE Transaction on Robotics and Automation 22 (4) (2006) 763–775.

[40] H. Janocha, C. Stiebel, New approach to a switching amplifier for piezoelectric actuators, in: Proceedings of ACTUATOR 98, 6th Int. Conf. on New Actuators, Bremen, Germany, 1998, pp. 189–192.

[41] D. Campolo, M. Sitti, R. S. Fearing, Efficient charge recovery method for driving piezoelectric actuators with quasi-square waves, IEEE Trans. on Ultrasonics, Ferroelectrics and Frequency Control 50 (3) (2003) 237–244.

[42] K. Kuhnen, H. Janocha, D. Thull, A. Kugi, A new drive concept for high-speed positioning of piezoelectric actuators, in: Proceedings of the 10th Int. Conf. on New Actuators, Germany, 2006, pp. 82–85.